

THESIS

A COMPARISON OF MCNP MODELING AGAINST EMPIRICAL DATA FOR THE  
MEASUREMENT OF GAMMA FIELDS DUE TO ACTINIDE OXIDES IN A GLOVEBOX

Submitted by

David Wright Adams

Department of Environmental and Radiological Health Sciences

In partial fulfillment of the requirements

For the Degree of Master of Science

Colorado State University

Fort Collins, Colorado

Fall 2012

Master's Committee:

Advisor: Alexander Brandl

Thomas E. Johnson

James E. Lindsay

## ABSTRACT

### A COMPARISON OF MCNP MODELING AGAINST EMPIRICAL DATA FOR THE MEASUREMENT OF GAMMA FIELDS DUE TO ACTINIDE OXIDES IN A GLOVEBOX

Los Alamos National Laboratory (LANL) is a facility that conducts research in the fields of global security, astrophysics, nuclear energy, and materials science. At Technical Area 55 (TA-55) actinide oxides used for experimental nuclear fuel research are placed in gloveboxes to be manipulated by glovebox operators. The actinide oxides are radioactive and emit gamma rays which impact the glovebox operator. Although proper precautions protect workers from unnecessary dose, the measurement and characterization of the gamma fields are useful in deciding if multiple dosimetry may be necessary as per standards at the lab and national standards. Experimental measurements were made by radiation protection personnel of TA-55 at the glovebox containing different actinide oxides. Thermoluminescent dosimeters (TLDs) were utilized to determine the dose to workers at the glovebox. A lead apron covered some of the TLDs while others were left unshielded to simulate shielded and unshielded portions of the body. Monte Carlo N-Particle Code Version 5 (MCNP5) was used to model and simulate the experimental setup at TA-55 to determine the efficacy of the lead apron and to determine the spatiality of the dose distribution as required to determine whether multiple dosimetry is necessary or not. Multiple dosimetry was found to not be required given that the TLD's are worn on the chest, at the location of highest dose.

# TABLE OF CONTENTS

	<u>Page No.</u>
1.0 Introduction, Theory, and Background.....	1
a. Los Alamos National Laboratories Technical Area-55 .....	1
b. Theory .....	2
c. Previous Work .....	4
2.0 Methods and Materials.....	6
a. LANL Methods and Materials .....	6
b. MCNP Methods and Materials .....	15
3.0 Results.....	22
a. Introduction of the Results.....	22
b. LANL Radiation Protection Results .....	25
c. MCNP Results .....	27
4.0 Discussion.....	45
a. Spatiality of the Dose Distribution .....	47
b. Efficacy of the Lead Apron.....	49
5.0 Conclusions.....	51
6.0 References.....	55
7.0 Appendix A: MCNP Input With Americium Oxide Source.....	57

## **1.0 INTRODUCTION, THEORY, AND BACKGROUND**

### **a. LOS ALAMOS NATIONAL LABORATORIES TECHNICAL AREA-55**

Los Alamos National Laboratory was first established during the Manhattan Project, as a research facility for the designers, engineers, physicists, and other professionals working to create the first atomic bomb. Located in the hills above Santa Fe, New Mexico, at 2231 meters above sea level, today Los Alamos' mission has evolved to not only support the United States' nuclear weapons program, but to also maintain divisions in such fields as global security, astrophysics, materials sciences, and nuclear energy.

Los Alamos National Laboratory (LANL) utilizes glovebox lines for work on actinide-metal oxides such as plutonium, neptunium, americium, and uranium in the form  $XO_2$  in the Plutonium Facility, in Technical Area 55 (TA-55). Here, actinides are converted to fuel pellets for research and development. These metal oxides can be dangerous to handle as the actinides are radiological and chemical hazards. Although the actinides are primarily alpha particle emitters, photons and neutrons are also emitted from these metals. Neutrons and photons of sufficient energy can permeate the thin layers of steel, lead, borosilicate glass, and Hypalon™ used for protection in the gloveboxes, contributing to the dose of workers at LANL.

To limit dose to workers at LANL, protective equipment is worn. Because of the radiological conditions at TA-55, workers often, though not always, wear a Roland lead apron with 0.5 mm lead equivalency during actinide work. However, currently there is little scientific

justification for the workers to be burdened by wearing the lead apron, as there has been no study to determine the efficacy of dose reduction caused by the lead apron, nor has a study properly determined if multiple dosimetry is necessary. If the whole body dose is non-uniform with a greater-than 50% difference in dose distribution, multiple dosimetry is required by the laboratory. US federal regulations, in particular 10CFR835.2, state that “Whole body means, for purposes of external exposure, head, trunk (including male gonads), arms above the elbow, or legs above the knee” (CFR, 2012). The American National Standards Institute (ANSI), along with the Health Physics Society (HPS) (ANSI/HPS N13.41-2011) recommends supplemental dosimeters when the following two conditions are met: “1) The personal dose equivalent to any portion of the body has the potential to vary by 50% from the expected personal dose equivalent at the reference dosimeter location; and 2) the dose equivalent has the potential to exceed 10% of the limiting value when a significant component of the effective dose equivalent comes from a non-uniform radiation field.” The Radiation Protection team at TA-55 envisioned and designed a method to quantify the efficacy of wearing lead aprons during glovebox work and to determine if multiple dosimetry is necessary. The group’s findings suggested that lead aprons do lower dose rates to individuals, as is discussed below in the results section, but that multiple dosimetry was not necessary. These findings will be discussed later in Section 3.0.

## **b. THEORY**

Thermoluminescent dosimeters (TLDs) were used by Radiation Protection at LANL to determine dose rates. TLDs measure dose through the process of electron trapping. A TLD is mainly composed of a crystalline luminescent material, such as lithium fluoride or calcium

fluoride. However, impurities, or doping agents, are added to the crystal. When ionizing radiation interacts with the crystalline material, the electrons of the material become excited and move from the lower energy valence band to the conduction band, which is usually empty. Once the electrons enter this band, they will naturally drift back to the valence band which releases a photon. The doping agents, however, will cause electron traps to form. Electron traps will keep the electron from dropping back into the valence band. In order to remove the electrons from the traps, energy must be put into the crystal. This energy can come in the form of heat. Therefore, by heating the doped crystal and measuring the intensity of photons released by the crystal, radiation dose to the crystal can be accurately measured (Knoll, 2010).

The Monte Carlo N-Particle (MCNP) (Brown, 2002) code uses Monte Carlo methods to determine system behaviors, trends, and averages. MCNP calculations result from computationally generating individual particle behavior and tracking their behavior. A user inputs the type of particles emitted and to be transported through the model geometry, or a computationally generated space. This space is then filled with materials specified by the user. The code uses randomly generated energies, directions, and starting points for particles (unless specified by the user) and, using a statistical model, will track that particle's interactions until the particle is either absorbed or is killed off by the operator. Particles will interact with the materials inserted into the geometry by known physical interactions and their interaction probabilities as specified by user defined data libraries. The interactions of the primary particle may spawn new secondary particles which will then also be given a random energy and direction to be tracked through the model space. By doing this many times over, overall trends in the behavior of the particles, or averages, can be obtained. Therefore, by measuring the location, rates, and

interactions of the particle behavior, flux, and energy deposition through materials may be obtained. A measure of the particle behavior is known as a “Tally” in MCNP. These tallies are normalized to a per-particle average.

### **c. PREVIOUS WORK**

Monte Carlo methods are used in many health physics applications, including for the assessment of occupational exposures. Shultis et al. utilized Monte Carlo methods to estimate the dose rates on the surface of spent fuel casks (Shultis, 2000). Zoeger and Brandl examined the dose rate distribution from an arrangement of standard 200 L waste drums utilizing MCNP (Zoeger and Brandl, 2011). Although MCNP has been used in other studies for medical and reactor applications, among others, occupational exposures were the chief concern for this paper.

PF-4 is a plutonium facility and has previously had its photon radiation fields characterized by a method developed by Whicker et al. (Whicker et al., 1999). Their findings suggested that the distribution of the dose rates in PF-4 near gloveboxes was varied, however a TLD on the chest of the individuals working at the gloveboxes “provided for a reasonable estimate of the average dose equivalent to workers' torsos”. However, this study approximated the dose to a specific organ’s equivalent dose, and not a total “whole body” deep dose equivalent (DDE). The authors also recognized the “hardening” of the photons emitted by the actinide oxides in the glovebox by the shielding, so that mostly higher energy photons, those above approximately 100 keV reach the worker torso. Lower energy photons were transmitted to the outside of the glovebox only through the gloveports. In addition, the authors found that those

working in the area of the gloveboxes moved rapidly from one glovebox to another, and thus that the worker's dose should be estimated as a time-weighted average of the doses at each location (Whicker et al., 1999).

## 2.0 METHODS AND MATERIALS

### a. LANL METHODS AND MATERIALS

The four mixtures used in the experiment and the simulation were composed of more than one radioisotope. The uranium oxide, for example, is a mixture of 93%  $^{235}\text{U}$  and 7%  $^{238}\text{U}$ . Table 2-1 shows the radionuclide composition for each actinide-metal oxide.

**Table 2-1: Mass and content of the radionuclide mixtures for the actinide-metal oxides**

Actinide Oxide	$\text{NpO}_2$	$\text{PuO}_2$	$\text{AmO}_2$	$\text{UO}_2$
Mass (g)	25.65	25.85	24.99	25.52
Content	100% $^{237}\text{Np}$	94% $^{239}\text{Pu}$ ; 6% $^{240}\text{Pu}$	99.9% $^{241}\text{Am}$	93% $^{238}\text{U}$ ; 7% $^{235}\text{U}$

The plutonium and uranium oxides are of high purity, and are about 88% actinide by weight with the remaining 12% composed of oxygen and unidentified contaminants. The neptunium and americium oxides are of slightly lower purity, being 85% actinide by weight and 15% oxygen and other unidentified contaminants. Each of these radioisotopes emits a unique gamma spectrum, and each isotope has a unique half-life ( $T_{1/2}$ ). As distances and shielding are fixed, the gamma spectrum, half-life, and the amount of material present, are the determining factors for the dose in this glovebox scenario.

As shown in Table 2-1,  $^{237}\text{Np}$  as a metal oxide is present in isotopically pure form. However, the metal oxide has an unknown amount of contamination from both the decay of the  $^{237}\text{Np}$  and the process in which the neptunium oxide is created. The neptunium oxide consists of about 85%  $^{237}\text{Np}$ , while the rest of the complex consists of oxygen and the unknown contaminants. Neptunium is a manmade element created by the alpha decay of  $^{241}\text{Am}$ , or by the neutron capture by  $^{236}\text{U}$  and subsequent beta decay of  $^{237}\text{U}$  (Morss, 2011).  $^{237}\text{Np}$  is primarily an alpha emitter. However, a multitude of gammas are emitted from the decay of  $^{237}\text{Np}$  and its daughter products, including  $^{233}\text{Pa}$ . A vast majority of these gammas are low energy gammas, with a 29.37 keV gamma being emitted for 14% of the decays. Gammas above 100 keV occur at a high rate in the daughter product  $^{233}\text{Pa}$ , most notably a 312 keV gamma which occurs in 36% of the decays of  $^{233}\text{Pa}$ . The gamma energies and their respective probabilities for  $^{237}\text{Np}$  aged one year are shown in Figure 2-1.

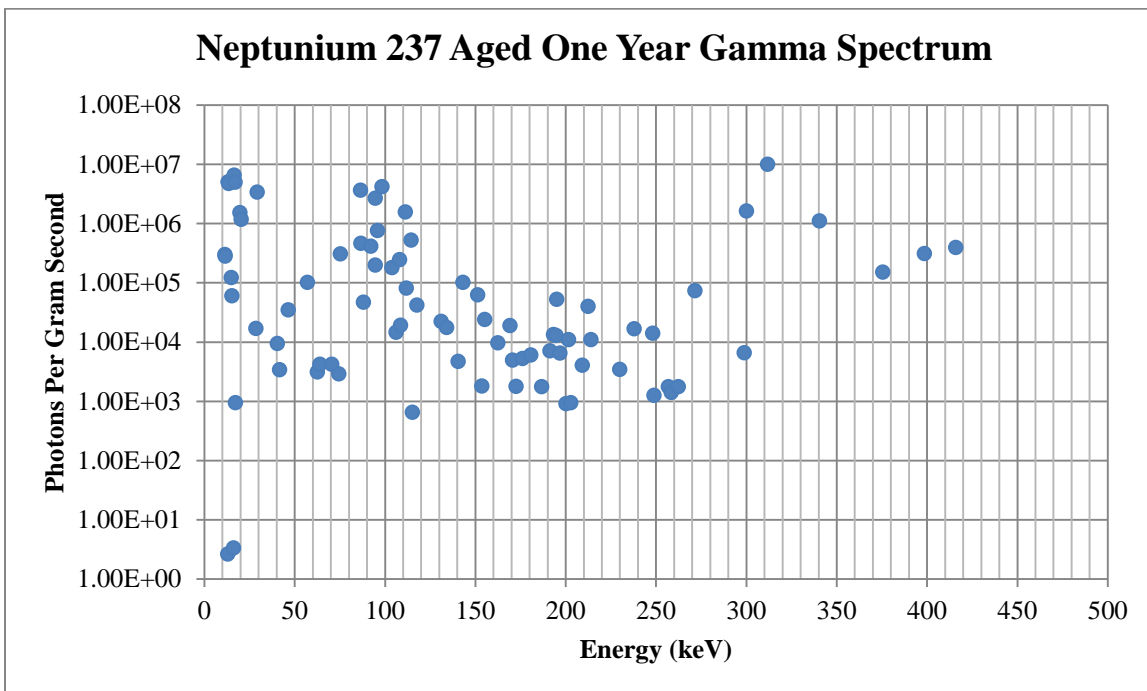
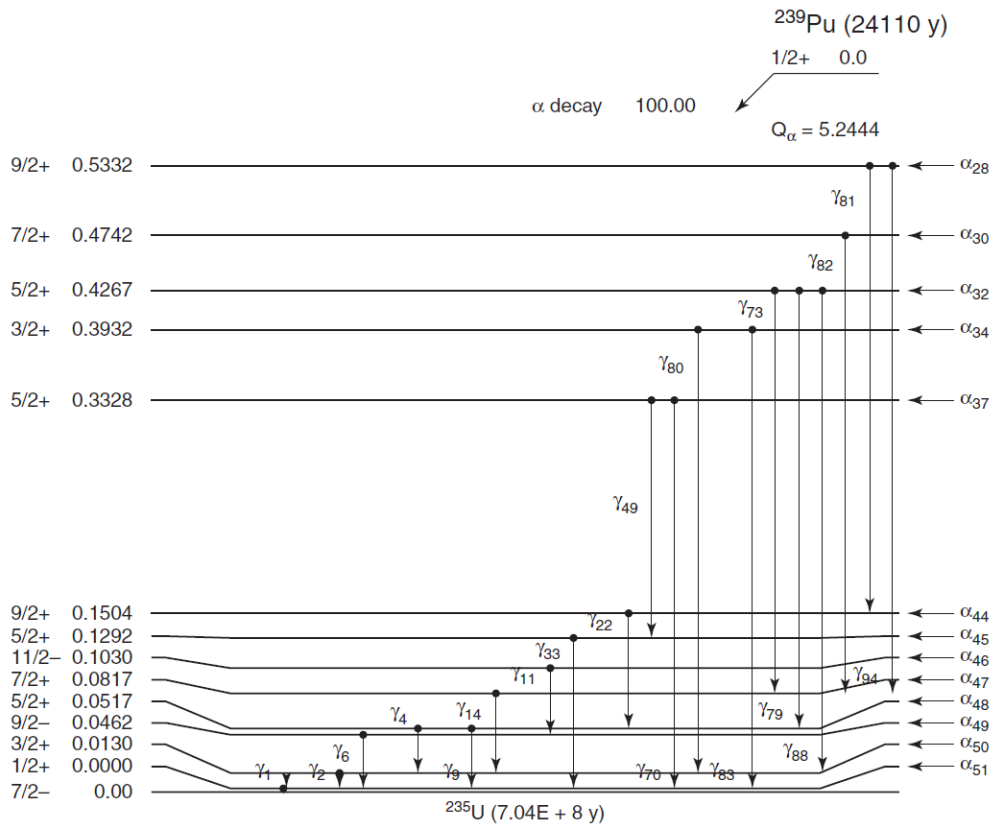


Figure 2-1: Unshielded  $^{237}\text{Np}$  Gamma Spectrum

Plutonium oxide that was used by RP-1 was composed of 94%  $^{239}\text{Pu}$ , and 6%  $^{240}\text{Pu}$ . The gamma spectrum of plutonium oxide is displayed in Figure 2-2. Plutonium is created when  $^{238}\text{U}$  captures a neutron and transmutes into  $^{239}\text{U}$  with a half-life of approximately 23.5 minutes, which beta decays into  $^{239}\text{Np}$ .  $^{239}\text{Np}$  subsequently beta decays with a half-life of about 2.36 days into  $^{239}\text{Pu}$ .  $^{239}\text{Pu}$  is primarily an alpha emitter. However, a 13 keV x-ray is emitted in about 7% of  $^{239}\text{Pu}$  decays, with a myriad of other gammas being emitted as well, as is displayed in Figure 2-2.



**Figure 2-2: Overview Demonstrating the Complexity of  $^{239}\text{Pu}$  Decay (BNL, 2012)**

$^{240}\text{Pu}$  is also primarily an alpha emitter and a low energy photon emitter. The mixture of  $^{239/240}\text{Pu}$  has a complex gamma spectrum as displayed in Figure 2-3. The plutonium oxide emits photons at a rate of about  $1.8 \times 10^6$  photons  $\text{g}^{-1} \text{s}^{-1}$ . However,  $^{240}\text{Pu}$  also decays by spontaneous fission in  $5.75 \times 10^{-6}\%$  of decays, or at a rate of about 500 fissions  $\text{g}^{-1} \text{s}^{-1}$  (Morss, 2011). The fission neutron rate produced by this process is 2.143 neutrons per fission. From the information in Table 2-1, the plutonium oxide has only 6%  $^{240}\text{Pu}$ . The mass of  $^{240}\text{Pu}$  is therefore about 1.37 grams, taking into account the mass of oxygen present. Therefore, we expect to observe greater than about 1465 neutrons per second.

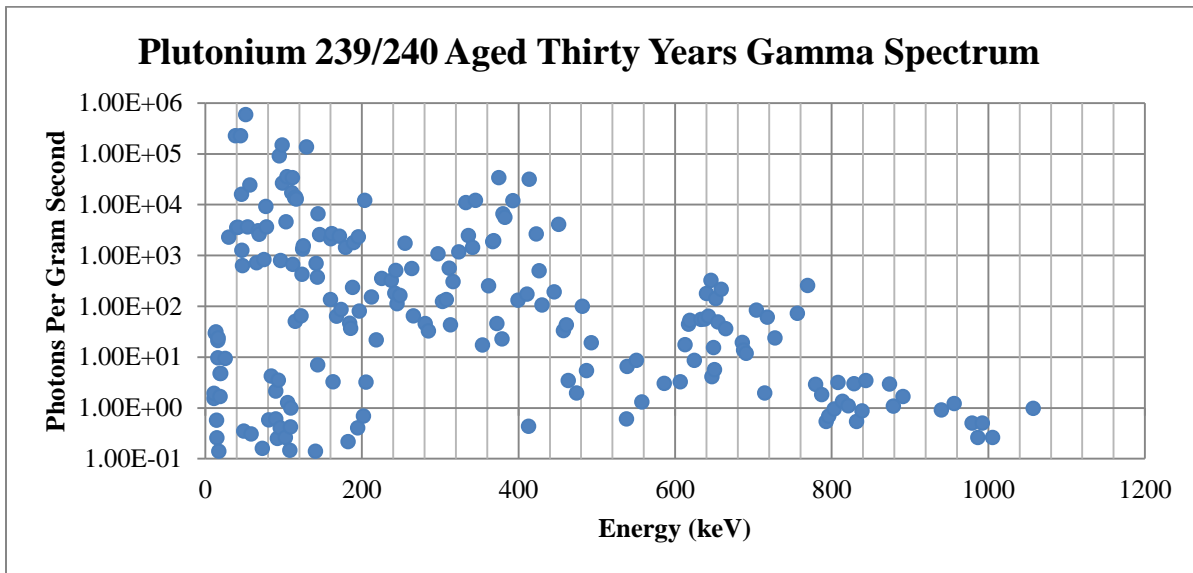


**Figure 2-3: Unshielded  $^{239/240}\text{Pu}$  Gamma Spectrum**

The americium oxide is composed primarily of  $^{241}\text{Am}$ . With a half-life of 432.7 y,  $^{241}\text{Am}$  is primarily an alpha emitter, though is also emits a distinctive 59.5 keV gamma ray in 35.7% of the decays and an array of other low energy gammas. However,  $^{241}\text{Am}$  and its daughters also emit gammas with energy greater than 100 keV in about 1% of the decays, as is displayed in Figure 2-5.

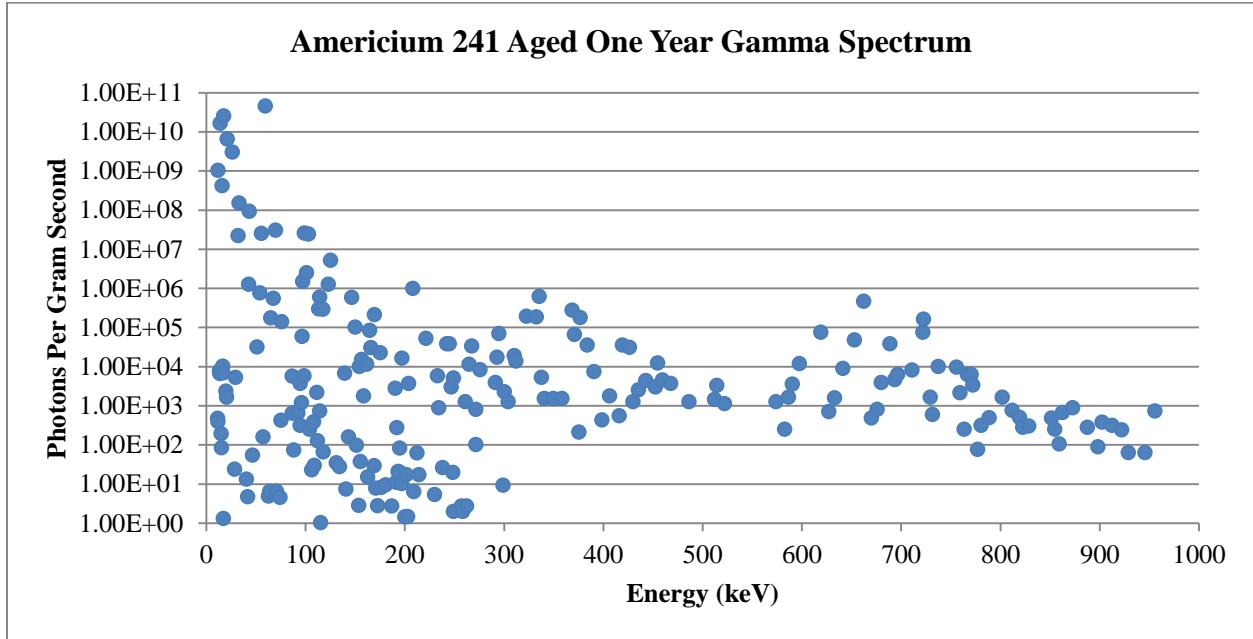


**Figure 2-4: Unshielded <sup>241</sup>Am Gamma Spectrum**

Highly enriched uranium oxide was also used in the glovebox experiment. The uranium is enriched to 93% <sup>235</sup>U and 7% <sup>238</sup>U. According to the NRC (CFR, for uranium enriched to a level greater than 72%), the specific activity (SA) of the enriched uranium is given by:

$$SA = [0.4 + 0.38(enrichment) + 0.0034(enrichment)^2] \times 10^{-6}$$

(Footnotes, CFR, 2012)

Therefore, for uranium enriched to 93% <sup>235</sup>U, the specific activity is equal to  $7.56 \times 10^{-5}$  Ci g<sup>-1</sup>. Enriched uranium emits measureable amounts of gamma radiation. The most distinctive gamma emissions from enriched uranium include a 185 keV gamma; emitted in 54% of the decays of

$^{235}\text{U}$ , and a 144 keV gamma emitted in 8% of the decays of  $^{235}\text{U}$  to  $^{231}\text{Th}$ . The gamma spectrum of the unshielded  $^{235/238}\text{U}$  is displayed in Figure 2-6.

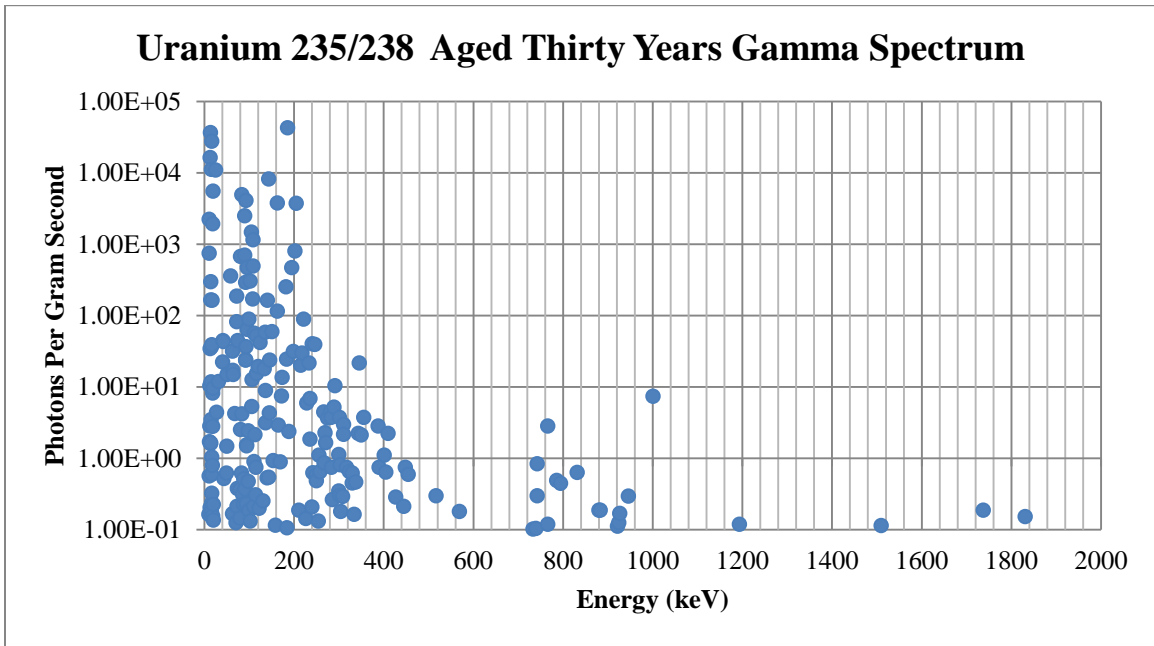


**Figure 2-5: Unshielded  $^{235/238}\text{U}$  Gamma Spectrum**

The glovebox itself is standard for this part of the plutonium facility and is composed of a shell of 7 gauge steel 0.47625 cm thick. The gloves are made of the polymer Hypalon®, a product of the DuPont™ Chemical’s Hypalon®, i.e.; chlorosulphanated polyethylene. The windows are made of borosilicate glass approximately 10 cm thick. An additional shield of leaded glass was placed on the window. This leaded glass is specified as LX-57b and is approximately ½ inch, 1.27 cm thick. LX-57b leaded glass is approximately 55% lead oxide by weight and an additional 5% barium oxide by weight. Inside of the glovebox, the actinide metal oxide material is in a powder form with a bulk density of approximately  $3 \text{ g cm}^{-3}$ , as is specified in a paper on the subject of production of americium oxide (Baybarz, 1960). The metal oxide powder is stored in a stainless steel cylinder approximately 1/16 inch (0.16 cm) thick.

Americium oxide, however, is stored in a container 3/16 inches thick, inside a lead wrap 1/16 inches (0.16 cm) thick which is inside a steel cylinder 1/16 inch (0.16 cm) thick. The cylinder sits approximately 30.5 cm from the front of the glovebox. The cylinder and the layers of shielding are shown in Figure 2-6.

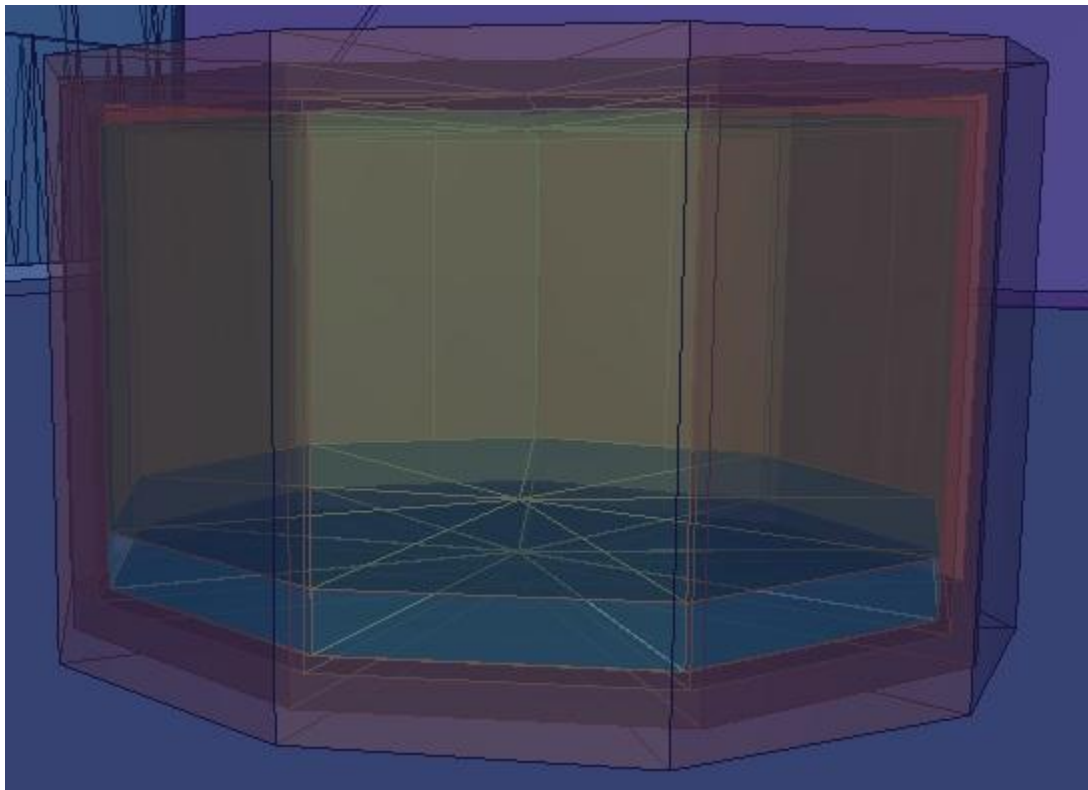


**Figure 2-6: Cylinder and Layers of Shielding Containing  $^{241}\text{Am}$  Generated by MCNP Visual Editor (Schwarz, 2011)**

The LANL specific Model 8823 Whole-Body Thermo-Luminescent Dosimeter (TLD) was used to measure the gamma radiation emitted by the different actinide oxides. This dosimeter contains two Harshaw/Bicron-NE TLD cards to determine photon, electron, and neutron dose. One card is used to calculate neutron dose, while the other is used to calculate photon and beta dose contributions. The Harshaw/Bicron-NE TLD cards contain four crystals,

each with variable shielding, to estimate deep dose, shallow dose, lens dose, beta dose, and neutron dose contributions. Examples of multi-element card dosimeters are displayed in Figure 2-7. Deep dose equivalent was the metric of concern for the purpose of lead apron shielding and multiple dosimetry, as this is what is required by the ANSI/HPS standard (ANSI/HPS N13.41-2011). A detailed description of how the Model 8823 measures dose is provided in Hoffman and Mallet (Hoffman and Mallet, 1999).

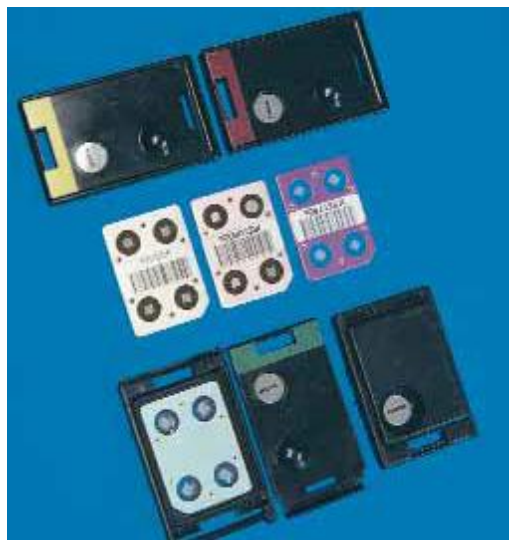


**Figure 2-7: Multi-element Card Dosimeters (Thermo Fisher Scientific ©, 2012)**

TLDs and an EPD were placed on a Lucite™ phantom which was covered with a Roland 0.5 mm leaded apron and positioned in front of the glovebox about a ½ inch (1.27 cm) away from the middle lead glass shielded window. Four TLDs were taped to the front of the phantom, and two TLDs and the EPD were taped to the back. Four TLDs were positioned on the leaded apron in approximately the same locations as those TLD's below. The leaded apron was placed over the phantom and positioned close to the glovebox to simulate an employee's position while working in a glovebox. EPDs were used to get a real time estimate of the dose being received as

well as to compare with the TLD results. The experimental setup ran for approximately 24 h for each material. The TLDs were submitted to the Health Physics Analysis Laboratory for processing. The average deep dose equivalent for TLDs for each location was reported as both shielded (under lead apron) and unshielded (TLDs positioned on top of lead apron) deep dose. The average for the two TLDs positioned on the back of the phantom was also reported for each material. The positions of the TLDs are displayed in Figure 2-8. The results were normalized to  $\text{mrem h}^{-1} \text{g}^{-1}$  for each material and the percent dose reduction was calculated. Figure 2-8 shows the experimental setup in the LANL plutonium facility.

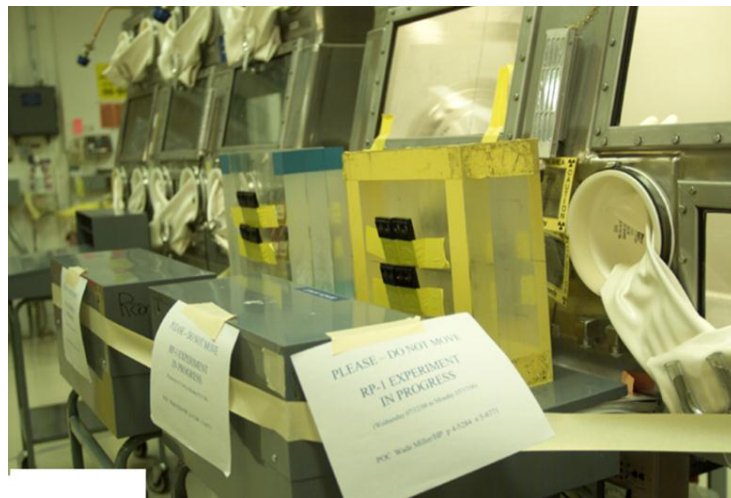


**Figure 2-8: Glovebox at TA-55 Room 126 with Lucite™ slab phantom and Model 8823 Whole-Body TLD's attached during RP-1 experiment**

## **b. MCNP METHODS AND MATERIALS**

Computer simulation calculations were done using MCNP — A General Monte Carlo N-Particle Transport Code, Version 5. This version of MCNP was installed using a Windows Installer on a computer with 4 GB of random-access memory (RAM) with an Intel® Core™ i3 central processing unit (CPU) running at 2.40 GHz with two cores and four logical processors.

In this study, flux was used as the metric of energy deposition to compare results from MCNP to actual energy deposition in TLDs. The International Commission on Radiological Protection (ICRP) (ICRP 1996) lists flux to air kerma factors for photons that may be used with MCNP. ICRP has also published air kerma to personal deep dose equivalent ( $H_p(10)$ ) factors to determine dose to man. The factors are shown graphically in Figure 2-9 and Figure 2-10. A direct conversion factor from photon fluence to  $H_p(10)$  in Sieverts (Sv) can be obtained by multiplying air kerma factors for each specific energy by the corresponding  $H_p(10)$  factors. The factors were used to produce results in Sieverts ( $H_p(10)$ ) for comparison with dosimetry results. After this step was added to the MCNP calculation, the tally produced an output in Sv per particle. The output was then multiplied by the activity of the source to arrive at a dose rate in Sv per second, which was then converted directly to millirem per hour.

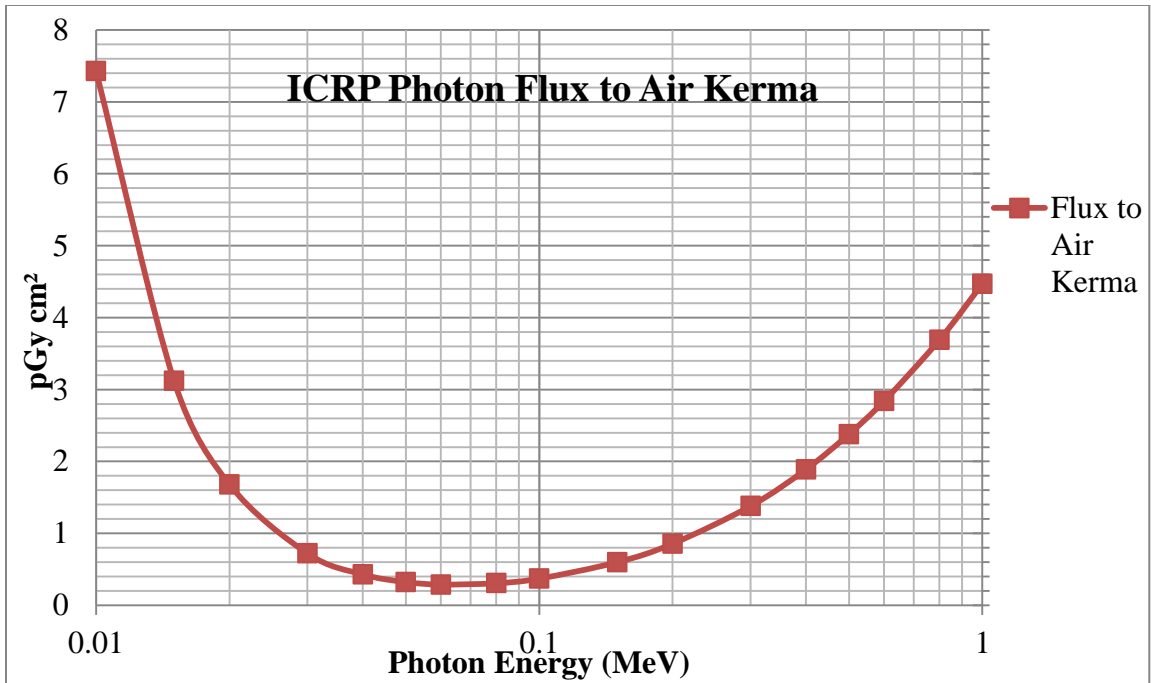


Figure 2-9: ICRP Photon Flux to Air Kerma Factors

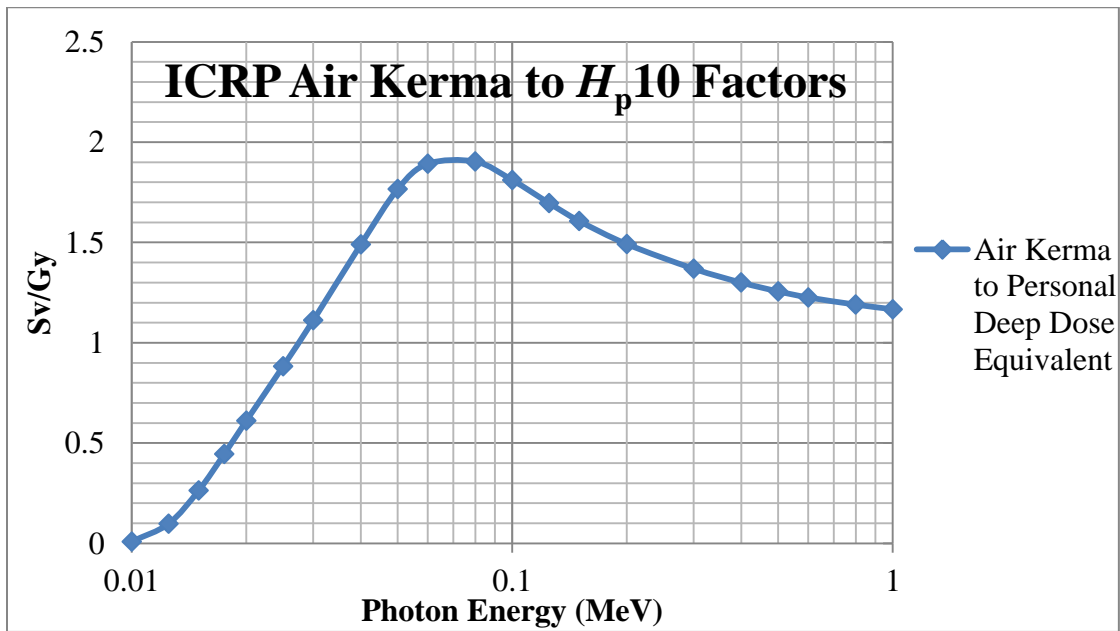
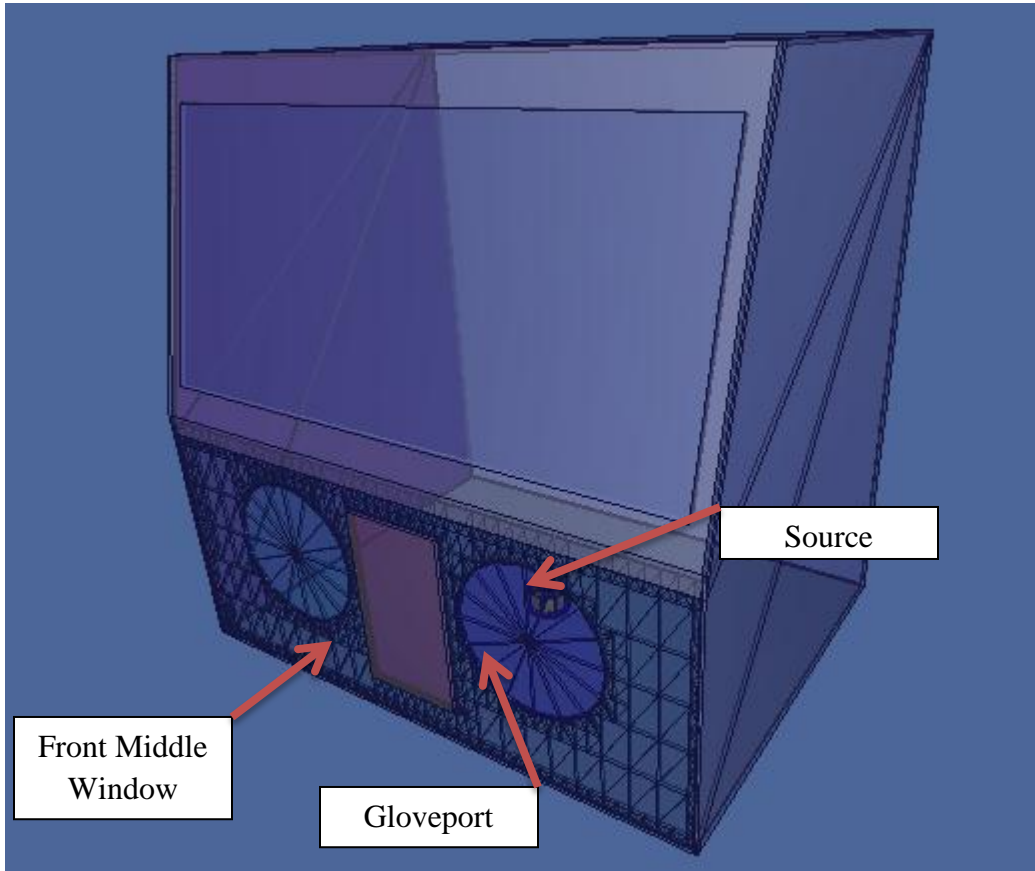


Figure 2-10: ICRP Air Kerma to Personal Deep Dose Equivalent

The glovebox model underwent several iterations before becoming the final build that was used for modeling. The final build is displayed in Figure 2-11.



**Figure 2-11: Room 126 Glovebox MCNP Model Generated by MCNP Visual Editor**

**(Schwarz, 2011)**

Figure 2-11 shows the glovebox without the TLD's, lead apron, and Lucite™ phantom. The geometry of the gloves was ignored and replaced with a fill of Hypalon® material to simulate the gloves, as the gloves can be pulled inside out and outside of the glovebox itself. The glovebox design was approximated using a multitude of sources, as the exact design specifications for the glovebox in which the RP experiment took place were not readily

available. For this study, the shielding of the front middle window of the glovebox was the singular most important piece of the geometry. The window is at a 10 degree angle from the lower part of the glovebox as specified in the design document. In Figure 2-12 the Lucite™ phantom with the modeled lead apron and the modeled and simplified TLD's is shown in their configuration in MCNP.

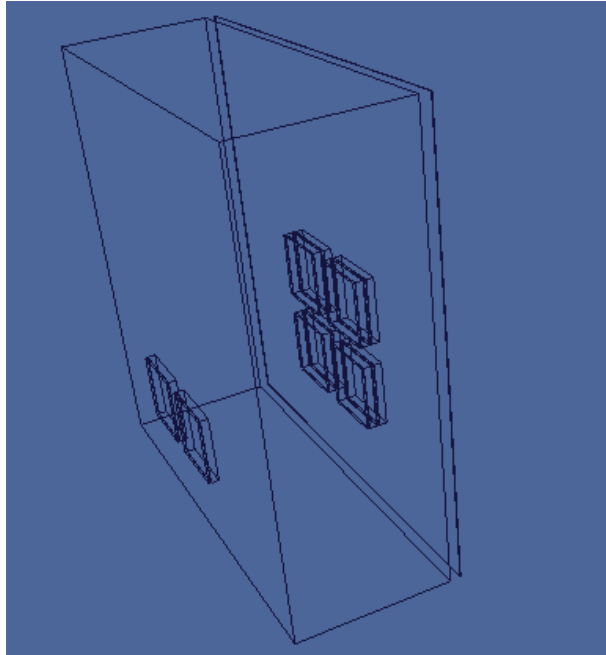


**Figure 2-12: Lucite™ phantom with TLD's and Lead Apron Placement Visible  
Generated by MCNP Visual Editor (Schwarz, 2011)**

The Monte Carlo N-Particle Code 5 (MCNP5) and Monte Carlo N-Particle X (MCNPX) codes were used to analyze the results of RP team's experiment. The glovebox, phantoms, a simplified model of the dosimeters, actinide-metal oxides, and containers of the actinide-metal oxides were modeled. The simplified model of the dosimeters was valid for use in this problem because the main components were modeled. The main components of the Model 8823 dosimeter for determining radiation dose from photons are the acrylonitrile butadiene styrene

(ABS) plastic cover and the two TLD chips used for determining radiation dose from the photon component of the dose (TLD-700 and TLD-400). The flux through the chips resulting in dose was modeled to estimate the  $H_p(10)$  dose. The photon spectra of the actinides were computed using the RadSrc (“Rad-Source”) code available from Lawrence Livermore National Laboratory (Hiller, 2007), which accounts for discrete gammas and bremsstrahlung as well as the radioactive decay of the source material. RadSrc also incorporates the gamma spectrum and bremsstrahlung from the daughters of the starting material.

Doses that were used for estimating the efficacy of the lead apron were calculated in MCNP using photon fluence tallies, F4 tallies, with fluence to personal deep dose equivalent (DDE) using correction factors from the International Commission on Radiological Protection (ICRP 1996). The TLD was approximated using solely the plastic shielding and the TLD elements of interest. F2 fluence tallies with 1 keV wide energy bins were used in order to obtain a photon spectrum of the un-scattered and scattered gammas emitted by the MCNP generated actinide source.

The distribution of the dose was estimated using F4 tallies as well. These tallies took the form of parallel thin detecting planes that were in front of the lead apron and behind the lead apron for the length of the “whole body” from the knee of the 5<sup>th</sup> percentile American female to the top of the head of the 95<sup>th</sup> percentile American male as defined by the National Aeronautics and Space Administration (NASA) Man-Systems Integration Standards (NASA, 1995). ICRP’s “Reference Man” was not considered for use as the necessary information is not provided in

Publications 89 or 23. These planes are shown in Figure 2-13 as the two long parallel black lines between the pink phantom on the left and the glovebox on the right.

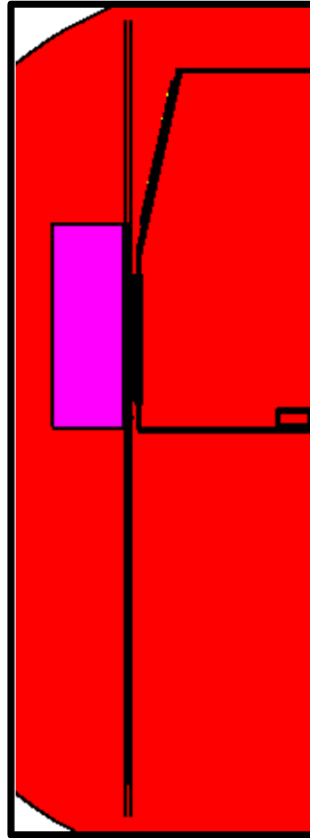


**Figure 2-13: The long black surfaces between the front of the glovebox and the phantom represent where dose rates were measured for the length of the “whole body”**

F4 tallies calculate the DDE by the flux of the particles in a specified cell. For this paper, the tallies specified were the TLD elements in the LANL Model 8823 dosimeter (Hoffman, 1998). These elements were modeled as a void in the simulation that used F4 tallies so that no secondary photons could be formed inside of the element. Had this not be done, secondary photons would contribute to the dose and overestimate the true absorbed dose. FM

multiplier cards were used to simulate the activity of the material which was provided by using the RadSrc Library.

F2 tallies with energy bins were utilized at three surfaces to estimate attenuation of gammas by the glovebox and the Roland 0.5 mm lead apron, as well as to characterize the gamma field, another requirement of the ANSI/HPS standard for multiple dosimetry (ANSI/HPS N13.41-2011). One F2 tally, labeled Tally 2, was placed at the surface of the interior of the middle glovebox window. Another, labeled Tally 12, was placed at the surface of the lead apron facing the glovebox. The third F2 tally, labeled Tally 22, was placed at the surface of the lead apron facing away from the glovebox, on the wearer's torso. The placement of the tallies was chosen to be ideal to measure the gamma flux which would directly influence the decision for lead apron utilization.

### **3.0 RESULTS**

#### **a. INTRODUCTION OF THE RESULTS**

The figures and tables in this section represent the data collected during the project. The Radiation Protection team's results are presented first in Tables 3-1 through 3-4. The findings of the Radiation Protection team are reported as total mrem integrated over a 24 h period from exposure to the actinide oxides in the glovebox. The findings were averaged over the 24 h time period to determine the average dose rate in  $\text{mrem h}^{-1}$  which was then used to find the decrease in dose rate caused by the lead apron. The decrease in dose rate also shows the difference in dose rate between the shielded chest region and the unshielded neck and head region of the "whole-body". Special attention was paid to the decrease in dose rate, as this is the metric which has the greatest influence on the decision of whether multiple dosimetry is necessary or not. If there is a difference greater than 50%, the argument for multiple dosimetry is supported for that radionuclide.

Following the Radiation Protection team's data are the original MCNP data from F4 flux tallies which are modified by flux to dose conversion factors. The data are reported in  $\text{mrem h}^{-1}$  in Tables 3-5 through 3-8. The relative error (error), variance of the variance (VOV), slope, and figure of merit (FOM) of the data are also reported. The tally's relative error is a measure of the computational precision. A reliable confidence interval may be formed if the error is less than 0.10 (X-5 Monte Carlo Team, 2003). The FOM is a measure of the efficiency of the calculation. The greater the FOM, the more efficient the problem is for calculating the tally of interest. The

consistency of the FOM is also important. An FOM for any tally should be consistent throughout the second half of the particle histories tallied during a particular Monte Carlo run. The FOM shows that a single particle “hit” on that tally does not drastically affect the result of the tally. A “hit” that does have a drastic effect on the tally is called a large history score. The number of particle large history scores must be minimized to improve confidence in the result. Instead, particles which affect that tally should be sampled consistently throughout the problem. The VOV is a metric of confidence which is particularly sensitive to large history scores. VOV’s should be below 0.1 and consistent throughout the second half of the problem. Slope is a measure of the spread of the upper tail of the distribution of history scores. Slope focuses on the largest 201 history scores. If the highest 100 history scores have a spread of less than 1%, then the slope is 10, or a perfect score. A slope of greater than 3 is considered necessary to satisfy the central limit theorem (CLT), wherein the scores have a normal distribution. If the slope is less than 3, the tally has not necessarily failed; however, the distribution used for the slope metric may not be representative of the actual distribution. The quantities of greatest interest in Tables 3-5 through 3-8 are the mean dose rates for the different tallies at the listed locations, under the heading “Mean”. These are directly related to the quantities described in the dose rates in Tables 3-1 through 3-4 in location relative to the glovebox on the phantom.

The spatial distribution of the dose as modeled using MCNP is also reported. The data in Figures 3-1 through 3-4 for the actinide oxides represent the deep dose equivalent in  $\text{mrem h}^{-1}$  over the length of the whole body as described in 10CFR835.2. The measure of the whole body length is the distance from the top of the knee of the 5<sup>th</sup> percentile American woman to the height of the top of the head of the 95<sup>th</sup> percentile American male as specified by NASA. The tables

which accompany the graphs (Tables 3-9 through 3-12) contain the dose information and the ratios of the doses at the different heights to the maximum dose. These graphs generally show two maxima for the dose rates. One is below the plane of the glovebox while the other is at the height of the front middle window.

The efficacy of the lead apron for the different actinide oxides is demonstrated in Tables 3-13 through 3-16. These data are directly comparable to the LANL data in Tables 3-1 through 3-4 for the decrease in dose rate caused by the attenuation of gammas in the lead apron. The efficacy of both the glovebox and the lead apron for attenuation and absorption of the photons emitted from the actinide oxides in the stainless steel cylindrical containers is demonstrated in the graphs which follow, Figures 3-5 through 3-8. Tally 2 calculates the energy spectrum of the gammas emitted from the steel container. Tally 12 collects the energy spectrum of the gammas transmitted through the front middle glovebox window. Tally 22 calculates the energy spectrum of the gammas transmitted from the lead apron which would influence the dose to an individual behind the lead apron. Tally 22 is of particular interest as the loss of gammas caused by the lead apron absorption of the gammas is equal to the difference between Tally 22 and Tally 12. Tally 12 affects those tallies in front of the lead apron while Tally 22 affects those behind the lead apron.

**b. LANL RADIATION PROTECTION RESULTS**

**Table 3-1: The results of the TLD readings after a 24 h exposure to americium oxide in the glovebox**

<b>Americium <math>Hp(10)</math> Deep Dose TLD Results (mrem)</b>				
<b>Position</b>	<b>Phantom Front</b>	<b>Over Pb-Apron</b>	<b>Phantom Back</b>	<b>% Decrease in Dose Rate</b>
<b>TR</b>	<b>45</b>	<b>79</b>	<b>20</b>	
<b>TL</b>	<b>40</b>	<b>62</b>	<b>16</b>	
<b>BR</b>	<b>45</b>	<b>80</b>		
<b>BL</b>	<b>44</b>	<b>52</b>		
<b>Average</b>	<b>43.5</b>	<b>68.25</b>	<b>18</b>	
<b>mrem/h</b>	<b>1.81</b>	<b>2.84</b>	<b>0.75</b>	<b>36.26</b>

**Table 3-2: The results of the TLD readings after a 24 h exposure to neptunium oxide in the glovebox**

<b>Neptunium <math>Hp(10)</math> Deep Dose TLD Results (mrem)</b>				
<b>Position</b>	<b>Phantom Front</b>	<b>Over Pb-Apron</b>	<b>Phantom Back</b>	<b>% Decrease in Dose Rate</b>
<b>TR</b>	<b>105</b>	<b>115</b>	<b>27</b>	
<b>TL</b>	<b>109</b>	<b>133</b>	<b>24</b>	
<b>BR</b>	<b>91</b>	<b>109</b>		
<b>BL</b>	<b>24</b>	<b>115</b>		
<b>Average</b>	<b>82.25</b>	<b>118</b>	<b>25.5</b>	
<b>mrem/h</b>	<b>3.43</b>	<b>4.92</b>	<b>1.06</b>	<b>30.30</b>

**Table 3-3: The results of the TLD readings after a 24 h exposure to plutonium oxide in the glovebox**

<b>Plutonium <math>H_p(10)</math> Deep Dose TLD Results (mrem)</b>				
<b>Position</b>	<b>Phantom Front</b>	<b>Over Pb-Apron</b>	<b>Phantom Back</b>	<b>% Decrease in Dose Rate</b>
<b>TR</b>	<b>69</b>	<b>77</b>	<b>24</b>	
<b>TL</b>	<b>89</b>	<b>113</b>	<b>21</b>	
<b>BR</b>	<b>76</b>	<b>75</b>		
<b>BL</b>	<b>29</b>	<b>83</b>		
<b>Average</b>	<b>65.75</b>	<b>87</b>	<b>22.5</b>	
<b>mrem/h</b>	<b>2.74</b>	<b>3.63</b>	<b>0.94</b>	<b>24.43</b>

**Table 3-4: The results of the TLD readings after a 24 h exposure to uranium oxide in the globebox**

<b>Uranium <math>H_p(10)</math> Deep Dose TLD Results (mrem)</b>				
<b>Position</b>	<b>Phantom Front</b>	<b>Over Pb-Apron</b>	<b>Phantom Back</b>	<b>% Decrease in Dose Rate</b>
<b>TR</b>	<b>29</b>	<b>24</b>	<b>11</b>	
<b>TL</b>	<b>35</b>	<b>36</b>	<b>12</b>	
<b>BR</b>	<b>24</b>	<b>43</b>		
<b>BL</b>	<b>23</b>	<b>29</b>		
<b>Average</b>	<b>27.75</b>	<b>33</b>	<b>11.5</b>	
<b>mrem/h</b>	<b>1.16</b>	<b>1.38</b>	<b>0.48</b>	<b>15.91</b>

c. MCNP RESULTS

**Table 3-5: The results of the MCNP5 simulation of americium oxide in the glovebox**

Americium MCNP $1 \times 10^9$ Particles					
	Mean (mrem/h)	Error (mrem/h)	vov	Slope	FOM
Front Top Right Element 1	1.317100	0.015100	0.001400	3.600000	3.400000
Front Top Left Element 1	1.308300	0.015800	0.008500	3.000000	3.100000
Front Bottom Right Element 1	1.593600	0.012500	0.000500	3.600000	4.900000
Front Bottom Left Element 1	1.578300	0.012800	0.001800	3.100000	4.600000
*Behind Apron Top Right Element 1	1.227400	0.015900	0.004200	2.900000	3.000000
Behind Apron Top Left Element 1	1.192200	0.015700	0.001700	2.800000	3.100000
Behind Apron Bottom Right Element 1	1.496900	0.013100	0.000500	3.800000	4.500000
Behind Apron Bottom Left Element 1	1.446600	0.013400	0.000700	3.800000	4.200000
*Back Right Element 1	0.322680	0.027600	0.004200	2.100000	1.000000
Back Left Element 1	0.306450	0.027100	0.001500	2.400000	1.000000
Front Top Right Element 2	1.310000	0.014800	0.000700	3.800000	3.500000
*Front Top Left Element 2	1.362400	0.015200	0.003300	2.800000	3.300000
Front Bottom Right Element 2	1.631800	0.012400	0.000400	3.000000	5.000000
Front Bottom Left Element 2	1.581600	0.012500	0.000300	3.100000	4.900000
Behind Apron Top Right Element 2	1.224000	0.015800	0.003200	3.200000	3.100000
Behind Apron Top Left Element 2	1.255500	0.015900	0.002900	2.400000	3.000000
Behind Apron Bottom Right Element 2	1.477500	0.013600	0.002300	3.200000	4.200000
*Behind Apron Bottom Left Element 2	1.472800	0.013800	0.001700	2.900000	4.000000
*Back Right Element 2	0.297590	0.028100	0.002600	2.400000	0.970000
*Back Left Element 2	0.301960	0.027400	0.001600	2.500000	1.000000

**Table 3-6: The results of the MCNP5 simulation of neptunium oxide in the glovebox**

Neptunium MCNP $1 \times 10^9$ Particles					
	Mean (mrem/h)	Error (mrem/h)	vov	Slope	FOM
Front Top Right Element 1	4.136700	0.005400	0.002800	4.300000	14.000000
Front Top Left Element 1	4.125400	0.005100	0.000400	4.300000	16.000000
Front Bottom Right Element 1	4.627900	0.004500	0.000300	4.300000	21.000000
Front Bottom Left Element 1	4.515200	0.004500	0.000300	4.000000	20.000000
Behind Apron Top Right Element 1	3.673500	0.005800	0.001400	5.600000	13.000000
Behind Apron Top Left Element 1	3.602700	0.005600	0.000700	4.500000	13.000000
Behind Apron Bottom Right Element 1	4.122700	0.005000	0.000600	5.600000	16.000000
Behind Apron Bottom Left Element 1	4.045000	0.005400	0.001000	4.100000	15.000000
Back Right Element 1	0.724310	0.011000	0.002000	3.500000	3.500000
Back Left Element 1	0.713180	0.010700	0.001500	4.200000	3.600000
Front Top Right Element 2	4.110500	0.005200	0.003400	3.400000	15.000000
*Front Top Left Element 2	4.076700	0.005300	0.001200	2.900000	15.000000
Front Bottom Right Element 2	4.624900	0.004500	0.000500	5.200000	21.000000
Front Bottom Left Element 2	4.459700	0.004600	0.000200	4.300000	20.000000
Behind Apron Top Right Element 2	3.636000	0.005500	0.000400	10.000000	14.000000
Behind Apron Top Left Element 2	3.604600	0.005700	0.000700	6.400000	13.000000
Behind Apron Bottom Right Element 2	4.121100	0.005000	0.000500	5.900000	17.000000
Behind Apron Bottom Left Element 2	3.985900	0.005300	0.001000	4.600000	15.000000
*Back Right Element 2	0.749960	0.011000	0.002400	2.900000	3.500000
Back Left Element 2	0.718680	0.010500	0.000500	10.000000	3.800000

**Table 3-7: The results of the MCNP5 simulation of plutonium oxide in the glovebox**

Plutonium MCNP $1 \times 10^9$ Particles					
	Mean (mrem/h)	Error (mrem/h)	vov	Slope	FOM
Front Top Right Element 1	0.071869	0.010200	0.004800	3.300000	19.000000
Front Top Left Element 1	0.072106	0.009400	0.000300	4.600000	23.000000
Front Bottom Right Element 1	0.083584	0.008400	0.000500	5.600000	29.000000
Front Bottom Left Element 1	0.081044	0.008600	0.000600	4.400000	27.000000
Behind Apron Top Right Element 1	0.065744	0.010500	0.001700	3.200000	18.000000
Behind Apron Top Left Element 1	0.065851	0.010300	0.001200	3.900000	19.000000
Behind Apron Bottom Right Element 1	0.076795	0.009200	0.002100	4.000000	24.000000
Behind Apron Bottom Left Element 1	0.074018	0.009400	0.001000	3.900000	23.000000
Back Right Element 1	0.013797	0.019500	0.001400	2.900000	5.300000
Back Left Element 1	0.013838	0.019100	0.001100	5.300000	5.600000
Front Top Right Element 2	0.071408	0.009500	0.000500	3.400000	22.000000
Front Top Left Element 2	0.071887	0.010200	0.004200	3.100000	20.000000
Front Bottom Right Element 2	0.083022	0.008400	0.000600	3.000000	29.000000
Front Bottom Left Element 2	0.081365	0.008600	0.000500	4.300000	28.000000
Behind Apron Top Right Element 2	0.064574	0.010500	0.002000	3.000000	18.000000
Behind Apron Top Left Element 2	0.065027	0.010400	0.001500	4.300000	19.000000
Behind Apron Bottom Right Element 2	0.076283	0.009500	0.002400	3.100000	22.000000
Behind Apron Bottom Left Element 2	0.073423	0.009500	0.001500	4.000000	22.000000
Back Right Element 2	0.014177	0.019500	0.002200	3.400000	5.300000
Back Left Element 2	0.013944	0.019100	0.001200	3.400000	5.500000

**Table 3-8: The results of the MCNP5 simulation of uranium oxide in the glovebox**

Uranium MCNP $1 \times 10^9$ Particles					
	Mean (mrem/h)	Error (mrem/h)	vov	Slope	FOM
Front Top Right Element 1	0.001432	0.013500	0.013300	2.900000	6.700000
Front Top Left Element 1	0.001435	0.012200	0.002900	3.500000	8.200000
Front Bottom Right Element 1	0.001553	0.010800	0.001900	3.800000	10.000000
Front Bottom Left Element 1	0.001543	0.012000	0.008800	2.600000	8.500000
Behind Apron Top Right Element 1	0.001116	0.014700	0.003000	4.000000	5.700000
Behind Apron Top Left Element 1	0.001088	0.015800	0.004200	3.100000	4.900000
Behind Apron Bottom Right Element 1	0.001178	0.014000	0.003600	3.000000	6.200000
Behind Apron Bottom Left Element 1	0.001123	0.014400	0.003400	3.700000	5.900000
Back Right Element 1	0.000273	0.026700	0.010100	6.200000	1.700000
Back Left Element 1	0.000242	0.025600	0.003400	10.000000	1.900000
Front Top Right Element 2	0.001407	0.012100	0.002600	4.400000	8.300000
Front Top Left Element 2	0.001440	0.012000	0.001700	4.700000	8.500000
Front Bottom Right Element 2	0.001525	0.011200	0.008000	4.200000	9.700000
Front Bottom Left Element 2	0.001494	0.011800	0.007800	2.900000	8.800000
Behind Apron Top Right Element 2	0.001050	0.015600	0.004400	3.700000	5.000000
Behind Apron Top Left Element 2	0.001125	0.015200	0.007400	3.500000	5.300000
Behind Apron Bottom Right Element 2	0.001141	0.014500	0.004600	2.800000	5.800000
Behind Apron Bottom Left Element 2	0.001120	0.014000	0.003200	4.400000	6.300000
Back Right Element 2	0.000267	0.026200	0.006500	7.900000	1.800000
Back Left Element 2	0.000268	0.028100	0.019200	4.100000	1.500000

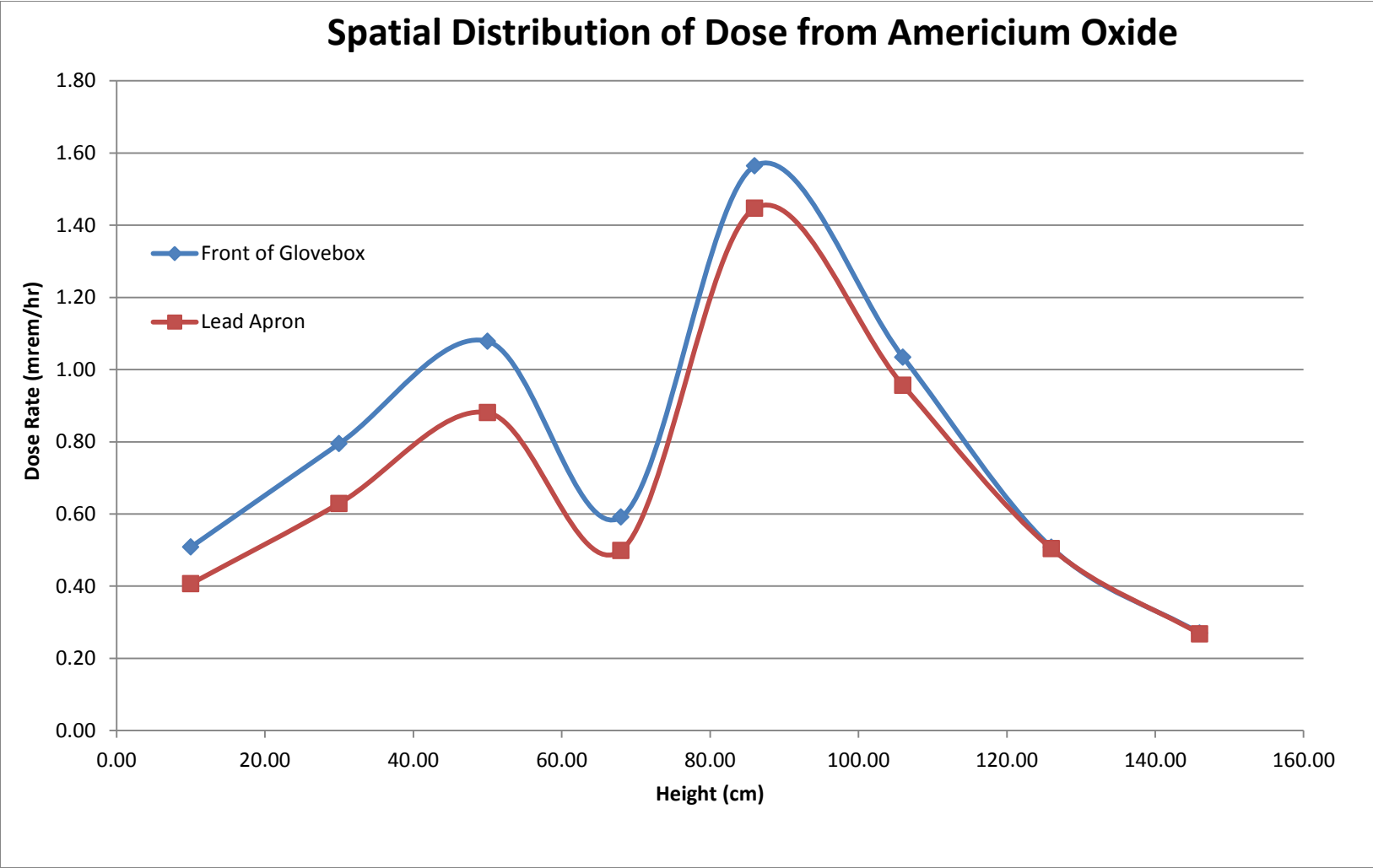


**Figure 3-1: Spatial Distribution of Dose from Americium Oxide**

**Table 3-9: Ratio of dose rates originating from americium oxide centered at the specified height to the highest observed dose rate**

Comparison of the Spatiality of Dose Distribution of Americium Oxide					
Front of Glovebox			Behind the Lead Apron		
Height (cm)	Dose Rate (mrem/h)	Ratio to Maximum Dose Rate	Height (cm)	Dose Rate (mrem/h)	Ratio to Maximum Dose Rate
10.00	0.51	32.49%	10.00	0.41	28.10%
30.00	0.79	50.81%	30.00	0.63	43.49%
50.00	1.08	68.96%	50.00	0.88	60.88%
68.00	0.59	37.82%	68.00	0.50	34.49%
86.00	1.56	100.00%	86.00	1.45	100.00%
106.00	1.03	66.14%	106.00	0.96	66.10%
126.00	0.51	32.44%	126.00	0.50	34.83%
146.00	0.27	17.25%	146.00	0.27	18.51%

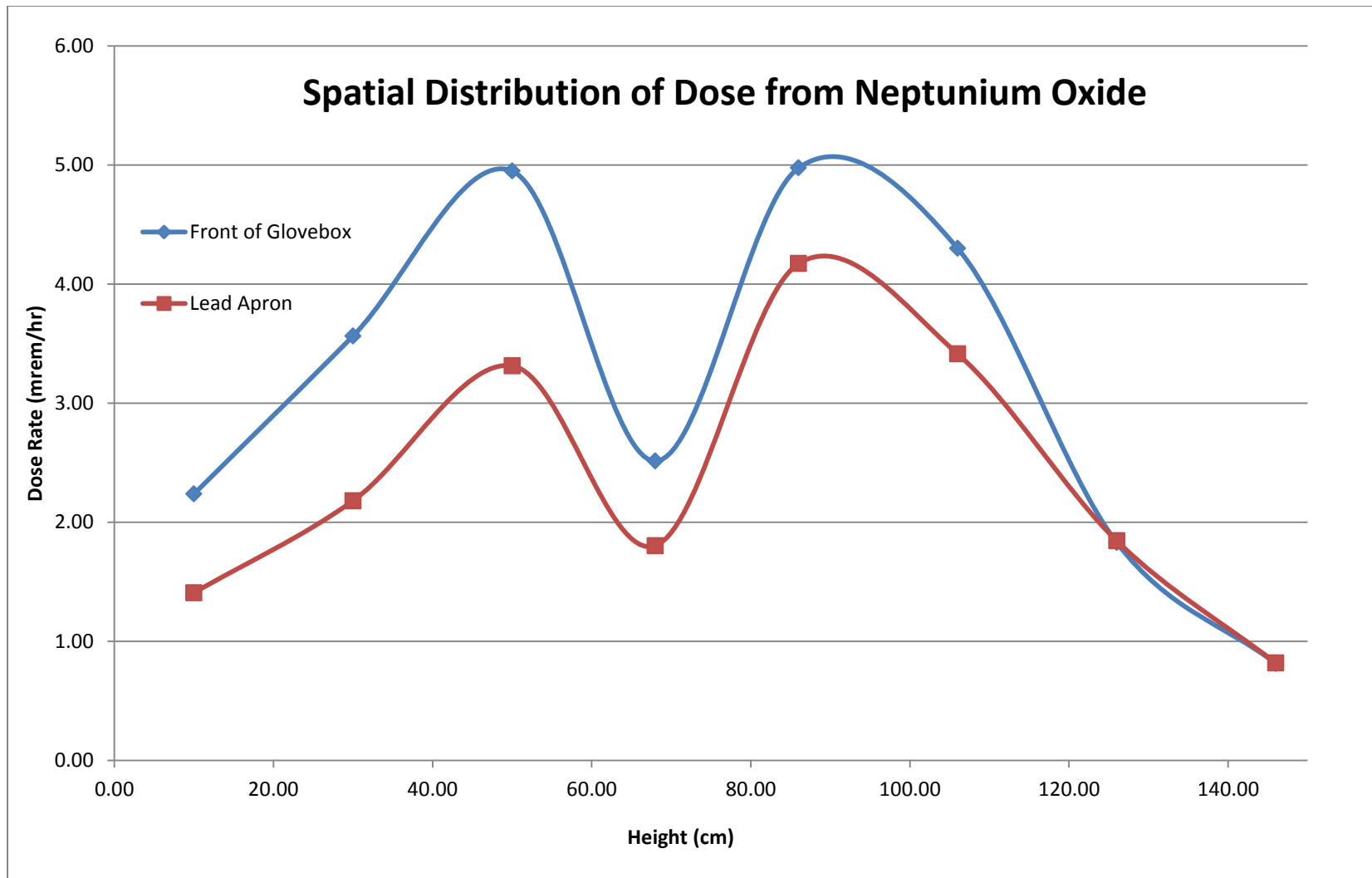


**Figure 3-2: Spatial Distribution of Dose from Neptunium Oxide**

**Table 3-10: Ratio of dose rates originating from neptunium oxide centered at the specified height to the highest observed dose rate**

Comparison of the Spatiality of Dose Distribution of Neptunium Oxide					
Front of Glovebox			Behind the Lead Apron		
Height (cm)	Dose Rate (mrem/h)	Ratio to Maximum Dose Rate	Height (cm)	Dose Rate (mrem/h)	Ratio to Maximum Dose Rate
10.00	2.24	44.97%	10.00	1.41	33.75%
30.00	3.56	71.64%	30.00	2.18	52.27%
50.00	4.95	99.48%	50.00	3.31	79.43%
68.00	2.51	50.53%	68.00	1.80	43.23%
86.00	4.98	100.00%	86.00	4.17	100.00%
106.00	4.30	86.42%	106.00	3.41	81.83%
126.00	1.83	36.76%	126.00	1.84	44.20%
146.00	0.81	16.36%	146.00	0.82	19.62%

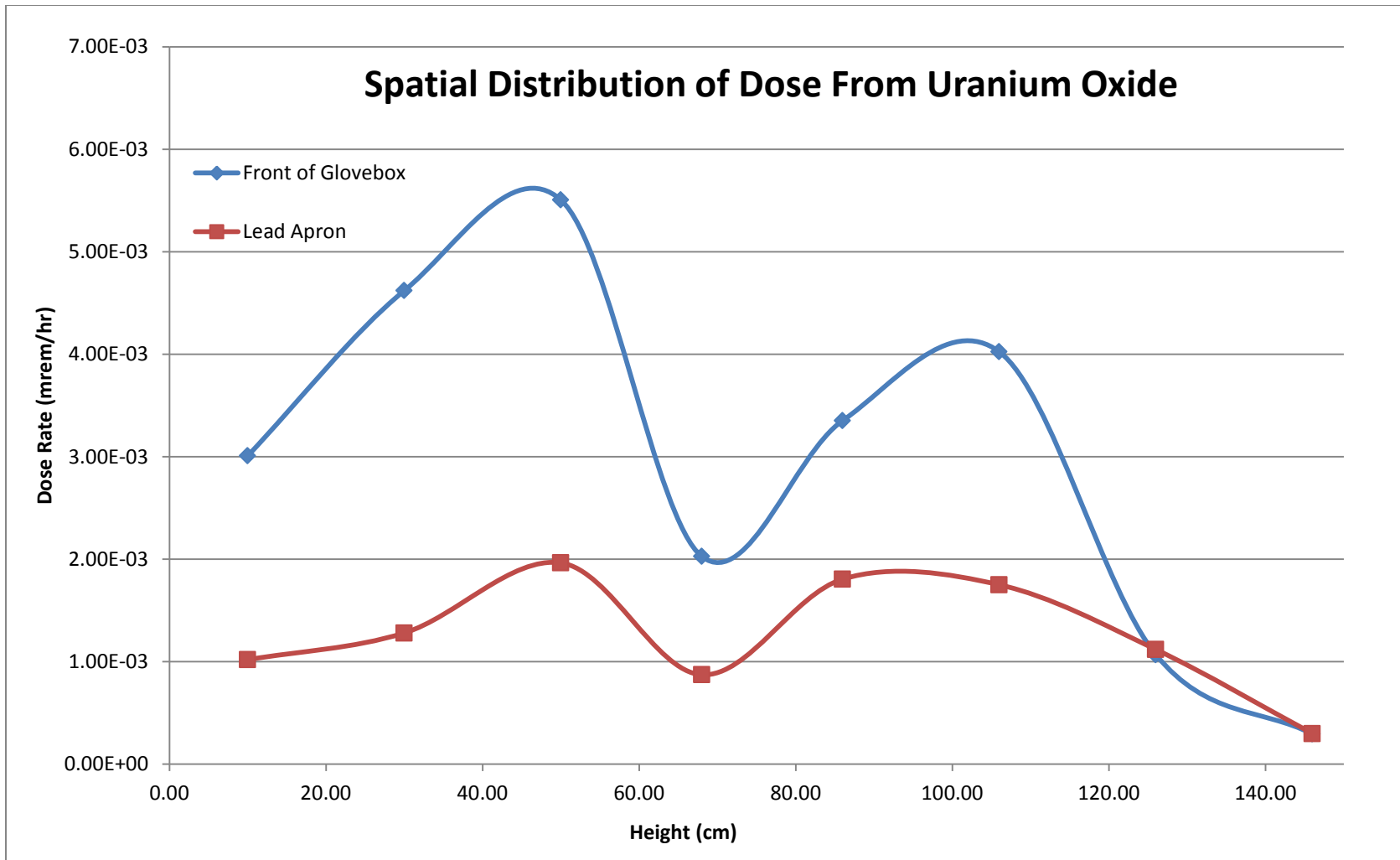
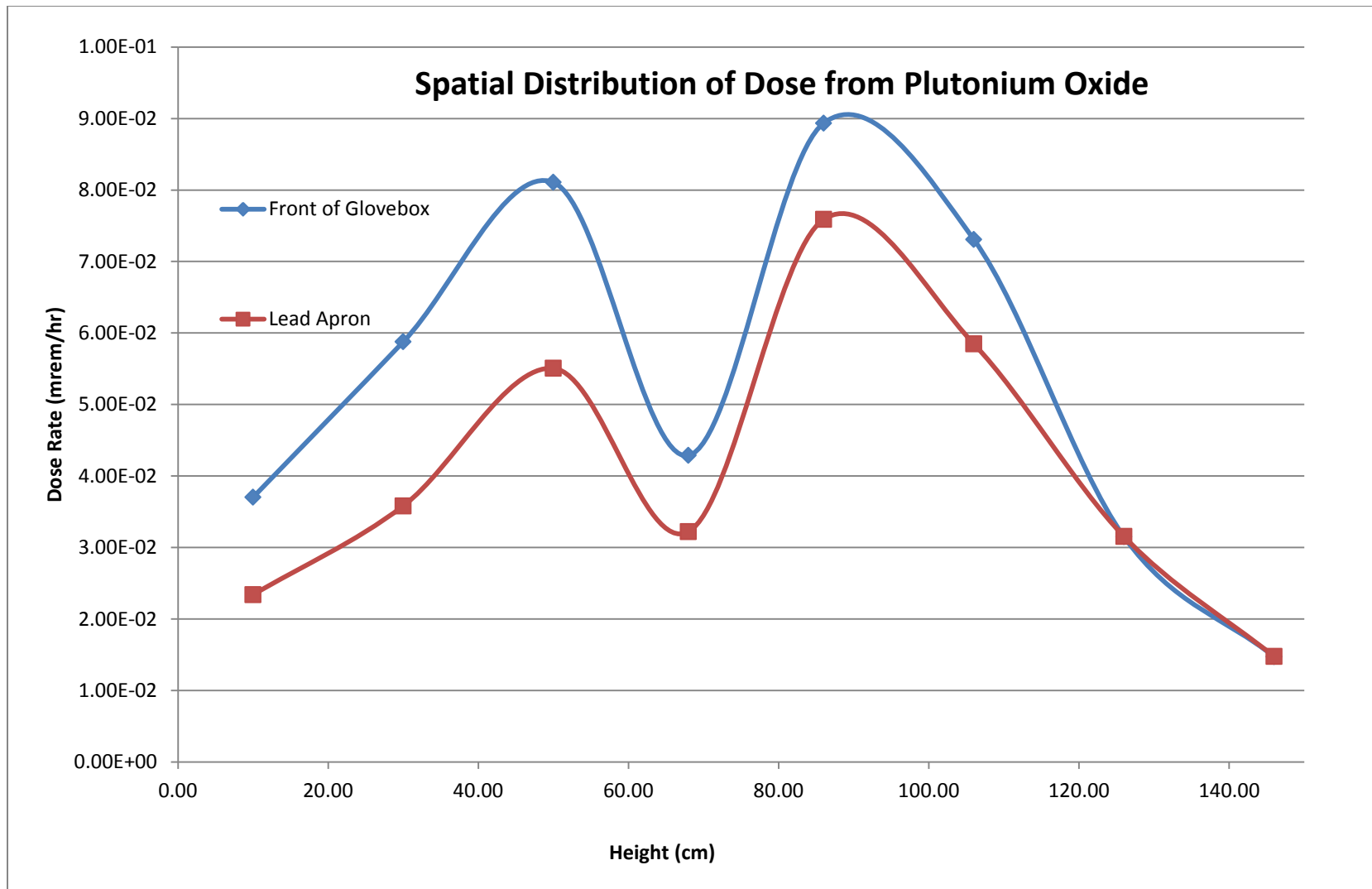


Figure 3-3: Spatial Distribution of Dose from Uranium Oxide

**Table 3-11: Ratio of dose rates originating from uranium oxide centered at the specified height to the highest observed dose rate**

Comparison of the Spatiality of Dose Distribution of Uranium Oxide					
Front of Glovebox			Behind the Lead Apron		
Height (cm)	Dose Rate (mrem/h)	Ratio to Maximum Dose Rate	Height (cm)	Dose Rate (mrem/h)	Ratio to Maximum Dose Rate
10.00	3.01E-03	54.64%	10.00	1.02E-03	51.87%
30.00	4.62E-03	83.92%	30.00	1.28E-03	65.17%
50.00	5.51E-03	100.00%	50.00	1.96E-03	100.00%
68.00	2.03E-03	36.82%	68.00	8.72E-04	44.39%
86.00	3.35E-03	60.89%	86.00	1.81E-03	91.92%
106.00	4.02E-03	73.08%	106.00	1.75E-03	89.11%
126.00	1.07E-03	19.40%	126.00	1.12E-03	56.95%
146.00	2.94E-04	5.33%	146.00	2.98E-04	15.19%



**Figure 3-4: Spatial Distribution of Dose from Plutonium Oxide**

**Table 3-12: Ratio of dose rates originating from plutonium oxide centered at the specified height to the highest observed dose rate**

Comparison of the Spatiality of Dose Distribution of Plutonium Oxide					
Front of Glovebox			Behind the Lead Apron		
Height (cm)	Dose Rate (mrem/h)	Ratio to Maximum Dose Rate	Height (cm)	Dose Rate (mrem/h)	Ratio to Maximum Dose Rate
10.00	3.70E-02	41.44%	10.00	2.34E-02	30.82%
30.00	5.88E-02	65.77%	30.00	3.58E-02	47.19%
50.00	8.11E-02	90.73%	50.00	5.51E-02	72.55%
68.00	4.29E-02	47.99%	68.00	3.22E-02	42.46%
86.00	8.94E-02	100.00%	86.00	7.59E-02	100.00%
106.00	7.31E-02	81.78%	106.00	5.85E-02	77.04%
126.00	3.15E-02	35.24%	126.00	3.15E-02	41.55%
146.00	1.47E-02	16.48%	146.00	1.47E-02	19.43%

**Table 3-13: Americium oxide results summary with the decrease in dose rate due to the 0.5 mm Roland Pb Apron**

Average Of Location Tallies: Americium Oxide				
Location	Mean (mrem/h)	Location	Mean (mrem/h)	% Decrease in Dose Rate
Front Top Right	1.31	Behind Apron Top Right	1.23	6.69
Front Top Left	1.34	Behind Apron Top Left	1.22	8.35
Front Bottom Right	1.61	Behind Apron Bottom Right	1.49	7.78
Front Bottom Left	1.58	Behind Apron Bottom Left	1.46	7.61
Back Right	0.31			
Back Left	0.30			

**Table 3-14: Neptunium oxide results summary with the decrease in dose rate due to the 0.5 mm Roland Pb Apron**

Average Of Location Tallies: Neptunium Oxide				
Location	Mean (mrem/h)	Location	Mean (mrem/h)	% Decrease in Dose Rate
Front Top Right	4.12	Behind Apron Top Right	3.65	11.37
Front Top Left	4.10	Behind Apron Top Left	3.60	12.13
Front Bottom Right	4.63	Behind Apron Bottom Right	4.12	10.90
Front Bottom Left	4.49	Behind Apron Bottom Left	4.02	10.52
Back Right	0.74			
Back Left	0.72			

**Table 3-15: Plutonium oxide results summary with the decrease in dose rate due to the 0.5 mm Roland Pb Apron**

Average Of Location Tallies: Plutonium Oxide				
Location	Mean (mrem/h)	Location	Mean (mrem/h)	% Decrease in Dose Rate
Front Top Right	0.072	Behind Apron Top Right	0.065	9.04
Front Top Left	0.072	Behind Apron Top Left	0.065	9.11
Front Bottom Right	0.083	Behind Apron Bottom Right	0.077	8.12
Front Bottom Left	0.081	Behind Apron Bottom Left	0.074	9.22
Back Right	0.014			
Back Left	0.014			

**Table 3-16: Uranium oxide results summary with the decrease in dose rate due to the 0.5 mm Roland Pb Apron**

Average Of Location Tallies: Uranium Oxide				
Location	Mean (mrem/h)	Location	Mean (mrem/h)	% Decrease in Dose Rate
Front Top Right	0.0014	Behind Apron Top Right	0.0011	23.72
Front Top Left	0.0014	Behind Apron Top Left	0.0011	23.02
Front Bottom Right	0.0015	Behind Apron Bottom Right	0.0012	24.67
Front Bottom Left	0.0015	Behind Apron Bottom Left	0.0011	26.14
Back Right	0.00027			
Back Left	0.00026			

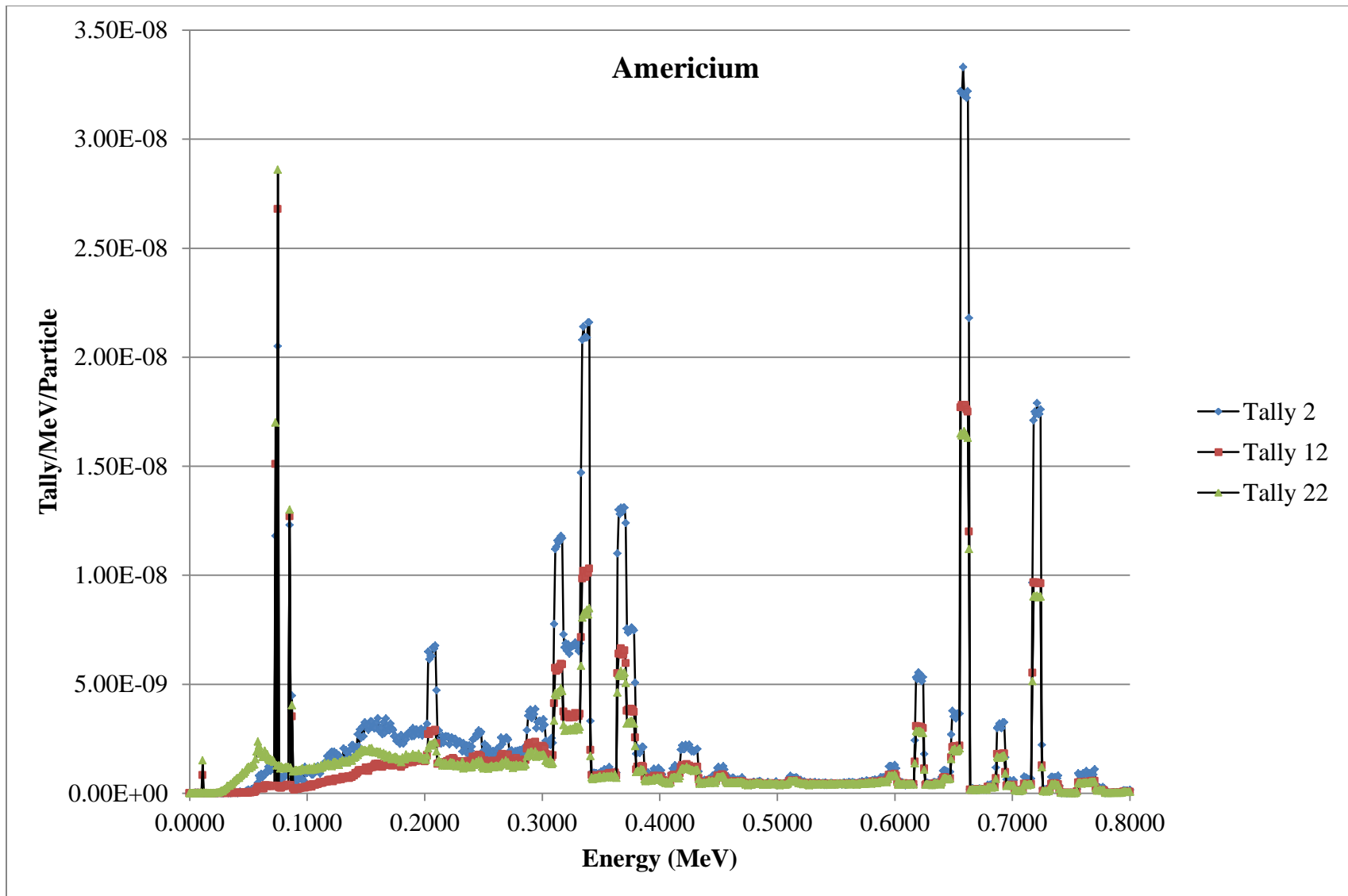


**Figure 3-5: Gamma flux at specified surfaces due to gammas originating at the MCNP generated americium source**

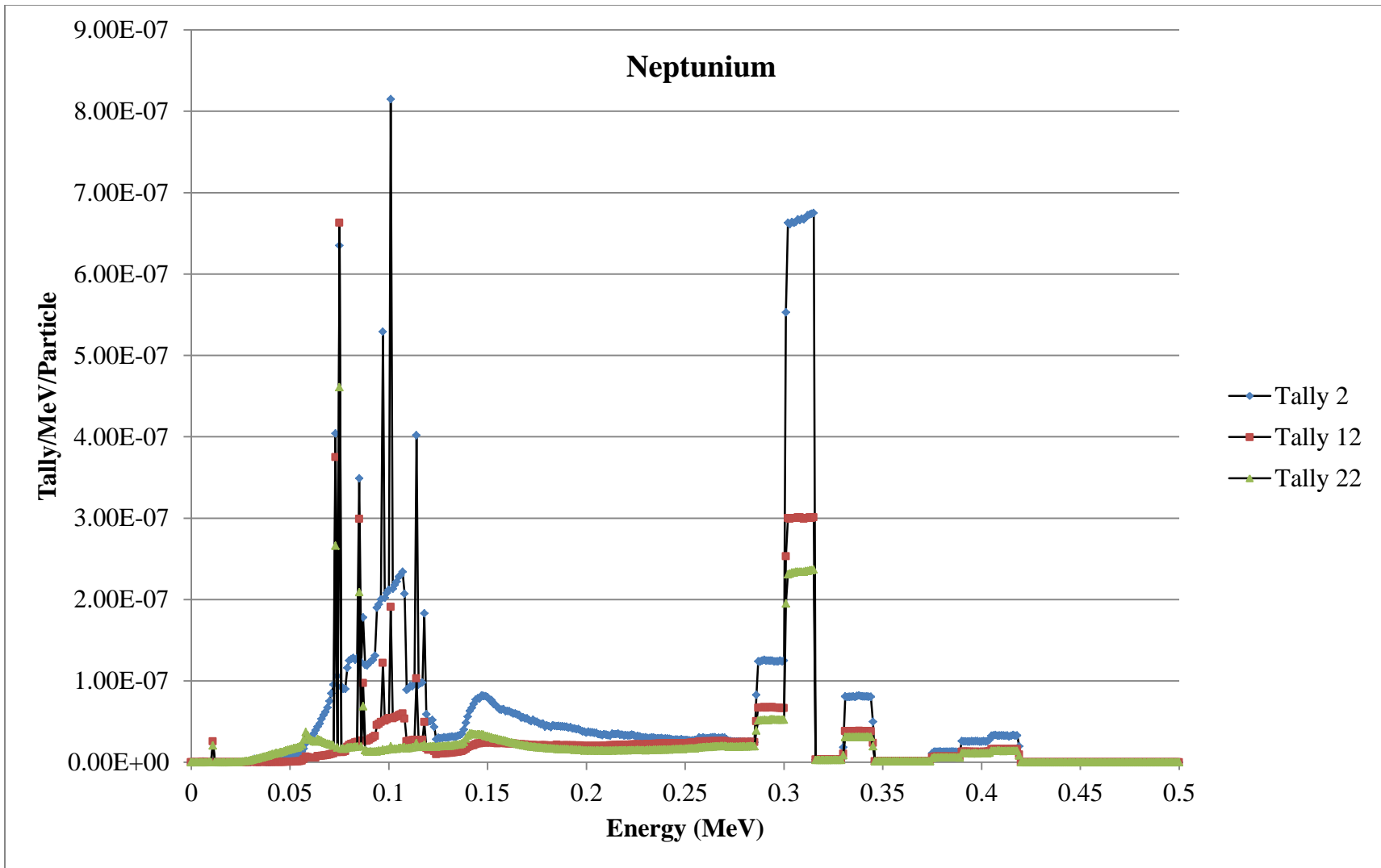


**Figure 3-6: Gamma flux at specified surfaces due to gammas originating at the MCNP generated neptunium source**

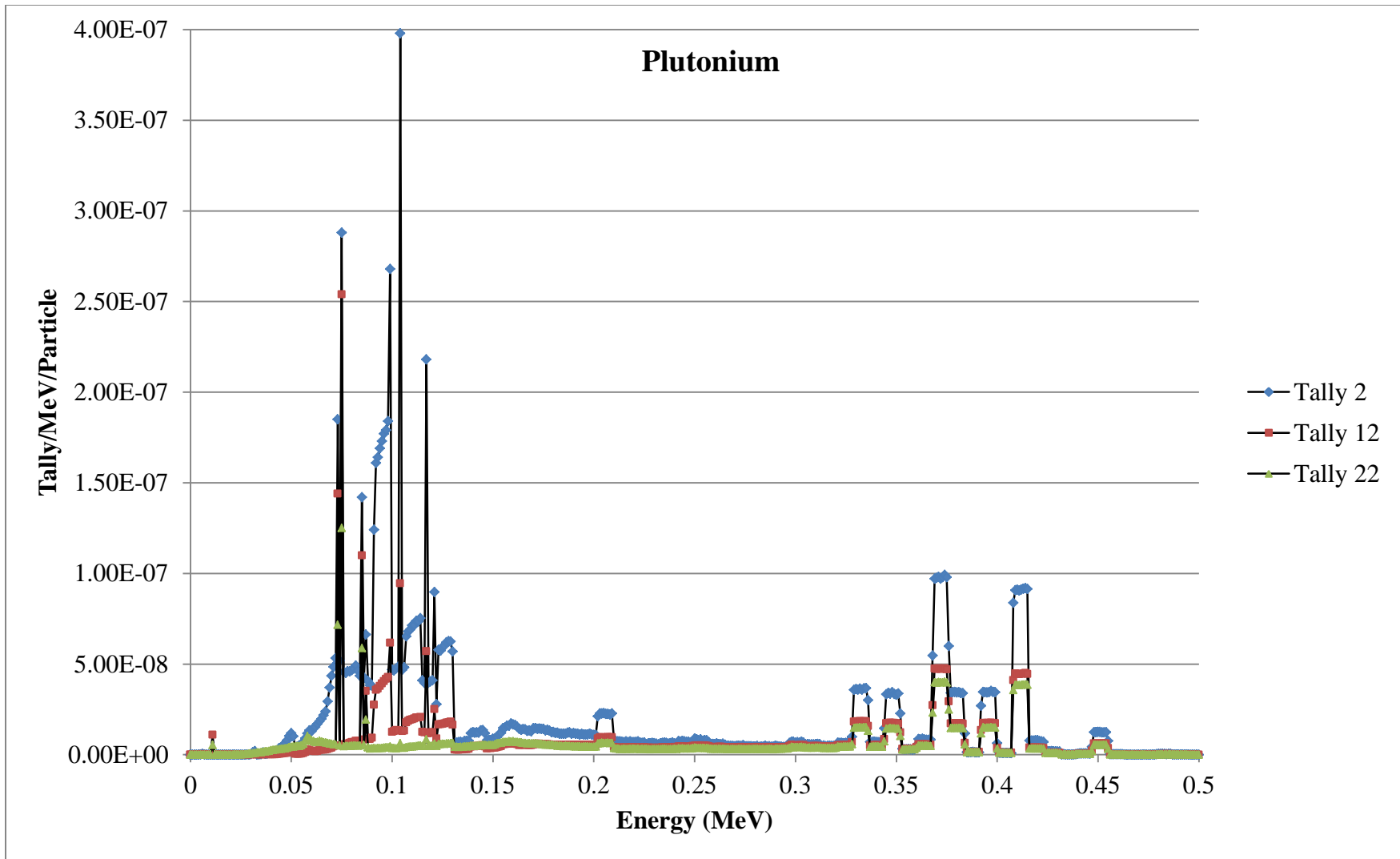


**Figure 3-7: Gamma flux at specified surfaces due to gammas originating at the MCNP generated plutonium source**

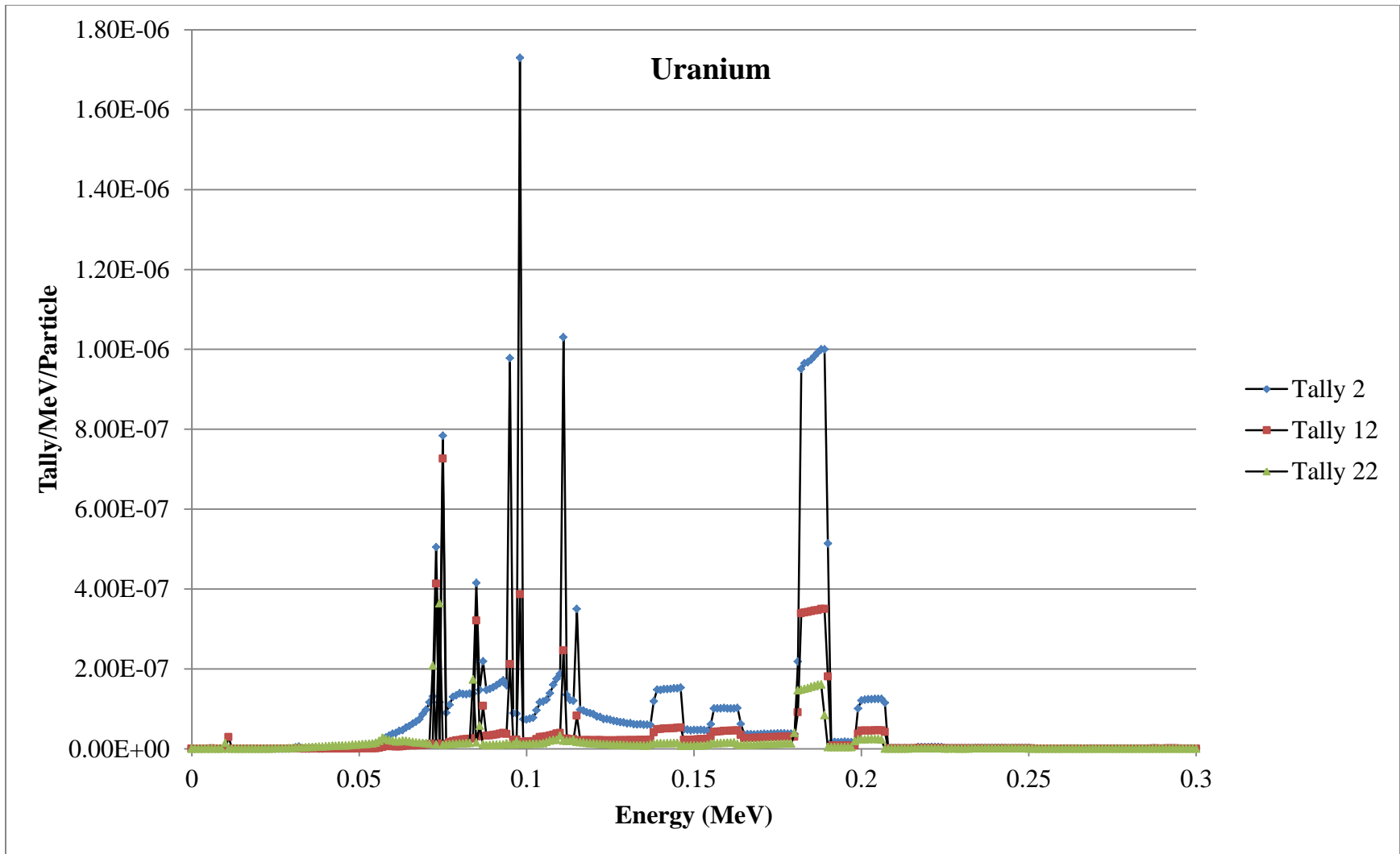


**Figure 3-8: Gamma flux at specified surfaces due to gammas originating at the MCNP generated uranium source**

## 4.0 DISCUSSION

The largest discrepancy in the data occurs for the  $^{235}\text{U}$  source. The dose rate was much higher than expected. The long half-life, subsequently low specific activity, amount of material, and the energies of the gammas emitted by  $^{235}\text{U}$  do not, by calculation, result in the dose rate at 30 cm observed using the TLD's at TA-55. The results of these calculations are in Table 4-1 and were calculated using gamma ray constants from Oak Ridge National Laboratory (ORNL) (ORNL, 1981). However, the LANL results do not match with any of the unshielded results as the sources are very well shielded. However, it is even more unexpected that a higher dose rate be obtained from the shielded material. This discrepancy in the data could be explained by high background, however, as would be expected in an actinide research laboratory.

The  $^{239/240}\text{Pu}$  source had a much lower resulting dose rate in MCNP than either the calculation below or the LANL result. The calculation below does not, as described earlier, take into account the shielding of the glovebox. The glovebox would be expected to shield a large portion of the gammas, and this can be visualized in Figure 3-7. Figure 3-7 shows that nearly all of the gammas below 250 keV were attenuated or absorbed by the glovebox and lead apron. Discrepancies in the age and isotopic mixture of the plutonium used by LANL and the  $^{239/240}\text{Pu}$  mix which was input into MCNP may account for the differences in the dose rate between the LANL result and the MCNP result. Small amounts of  $^{241}\text{Pu}$ ,  $^{241}\text{Am}$ ,  $^{242}\text{Pu}$  and  $^{240}\text{Pu}$  in the actual

source used by LANL may incur a substantial amount of dose to an individual in comparison to the large amount of shielded  $^{239}\text{Pu}$  and  $^{240}\text{Pu}$  typically found in mixtures of weapons grade Pu.

$^{241}\text{Am}$  results between the LANL results and MCNP were similar. The difference between the dose rates to the front TLD's for  $^{241}\text{Am}$  between the LANL and MCNP results was approximately 48%. This difference may also be due to the gloveports. The MCNP model had gloveports filled with Hypalon® as a disk. This approach resulted in an unrealistically thick glove, which acted as an attenuator for gammas. This is especially important when considering that  $^{241}\text{Am}$  emits low energy photons at a high rate, as well as low energy scattered photons. A thinner gloveport may have resulted in a larger number of these lower energy gammas being transmitted through the gloveport, resulting in a higher dose rate. The actual gloveport's Hypalon® thickness is 0.03 inches (LANL, 2008). The gloveport was filled with Hypalon® in the model, which resulted in a thickness of 0.19 inches (0.48 cm) of Hypalon®. Seams in the lead wrap used for  $^{241}\text{Am}$  and the metal container, also may have contributed to the LANL result. These discrepancies may also have affected the results for  $^{239}\text{Pu}$ .

**Table 4-1: Calculated dose rate data without shielding**

	$^{235}\text{U}$	$^{239}\text{Pu}$	$^{237}\text{Np}$	$^{241}\text{Am}$
Specific Activity(Ci/g)	2.10E-06	6.20E-02	6.90E-04	3.20E+00
Activity in Ci	4.62E-05	1.36E+00	1.47E-02	8.00E+01
Activity in MBq	1.71E+00	5.05E+04	5.43E+02	2.52E+06
mSv*m <sup>2</sup> /MBq*hr (ORNL,1981)	9.16E-05	8.14E-06	1.25E-04	8.48E-05
mSv/h at 1m	1.57E-04	4.11E-01	6.79E-02	2.13E+02
mSv/h at 30cm	1.74E-03	4.56E+00	7.54E-01	2.37E+03
mrem/h at 30cm	1.74E-01	4.56E+02	7.54E+01	2.37E+05

The results of both LANL and MCNP for the  $^{237}\text{Np}$  source in the glovebox were remarkably similar. There was only an 11% difference between the recorded TLD result of 4.92 mrem h<sup>-1</sup> and the MCNP result of 4.34 mrem h<sup>-1</sup>. The reason for the difference may be due to the energy spectrum of the gammas of  $^{237}\text{Np}$ . Figure 3-6 displays the gamma spectrum of  $^{237}\text{Np}$ . The gammas emitted by the  $^{237}\text{Np}$  source are more energetic than the gammas emitted by the other sources under consideration. The  $^{237}\text{Np}$  gammas transmit through the glovebox and shielding at a higher rate than gammas of lower energy and are the primary gammas of concern with respect to dose. The energies are also high enough so the thickness of the gloveports and small discrepancies in materials and design between the MCNP model and the actual glovebox do not greatly influence the transmission of the high energy gammas.

#### **a. SPATIALITY OF THE DOSE DISTRIBUTION**

The experimental findings showed that the dose distribution from the actinides observed did not require multiple dosimetry for individuals. In none of the cases did the observations show a 50% difference in dose between unshielded zones of the body and the area below the lead apron. However, this approach can only account for one aspect of two that will affect the dose rate to the area specified as the “whole body”.

The two factors that will affect the dose rate to different areas of the whole body are shielding and distance. The Radiation Protection group’s approach accounted for shielding, assuming that the result could also be applied to considerations for distance. However, the distance from the source has to be taken into account to fully account for the different areas of the “whole body” Without accounting for the dose rate dependences as a function of distance,

which can be much larger at the high and low areas of the “whole body”, only a partial description of the radiation field is made. According to the NASA Man-Systems Integration Standards, the height of the 95<sup>th</sup> percentile American male is 190.1 cm. The distance from the ground to the top of the knee of the 5<sup>th</sup> percentile sitting American female is 41.6 cm. Therefore, there are 148.5 cm from the knees to the top of the head that qualify as an area of consideration for the definition of the “whole body” by the USDOE.

The spatial distributions of dose, generated using MCNP, to an individual working at a glovebox with selected actinide oxides, are displayed in Figures 3-1 through 3-4. Ratios of different areas of the body are displayed for the actinide oxides in Tables 3-9 through 3-12. The horizontal axis (x-axis) points are the midpoints of the planes used for dose calculations. The dose distribution is spatially dependent, as shielding and distance changes throughout the area where doses to the “whole body” are concerned. Doses are highest below the base of the glovebox and at the front middle window. The results showed that over the area considered the “whole body” by the USNRC and DOE, dose rates to the whole body can be different by greater than 50%. The results displayed in Tables 3-9 through 3-12 are supported by the very similar results from Tables 3-5 through 3-8.

The front middle window consistently was the point of highest dose, except for in the case of uranium oxide, where the highest dose observed was below the base of the glovebox. Uranium’s gamma spectrum, displayed in Figure 3-8, shows that the energies of the gammas emitted are lower than those from the other source materials. Therefore, the reason the dose rate is higher below the bottom plane of the glovebox than at the window is because of increased scattering in air of the low energy gammas which are affecting the tally below that plane. The

data in Figure 3-3 show that the dose rate decreases significantly behind the lead apron both in front of the middle window and below the glovebox. The dose rates behind the lead apron are nearly equal, showing that the energies of the gammas below the lead apron are lower than those emitted from the front glovebox window. Figures 3-1 through 3-4 each show this same trend wherein the lead apron causes a greater loss of dose rate below the plane of the glovebox than of the dose rate from the front window. This decrease in dose rate caused by the lead apron below the lower plane of the glovebox supports the assessment that the dose rate below the plane of the glovebox is, at least partially, caused by scattered low energy gammas.

#### **b. EFFICACY OF THE LEAD APRON**

The Roland 0.5 mm lead equivalent lead apron decreased dose rates to workers due to the actinides in the glovebox. The lead apron will attenuate photons of all energies as can be identified in the differences between Tally 12 and Tally 22 in Figures 3-5 through 3-8. However, the lead apron did increase the number of photons between 60 keV and 150 keV in the case of Neptunium, which can be seen from the Compton peaks in Figure 3-6. The effect of the lead apron at these energies is directly influenced by lead's cross-section for photons of these energies, which is about 80 barns, as displayed in Figure 4-1. Figure 4-1 effectively demonstrates that, in general, gammas of higher energy are not attenuated as effectively as those of lower energy.

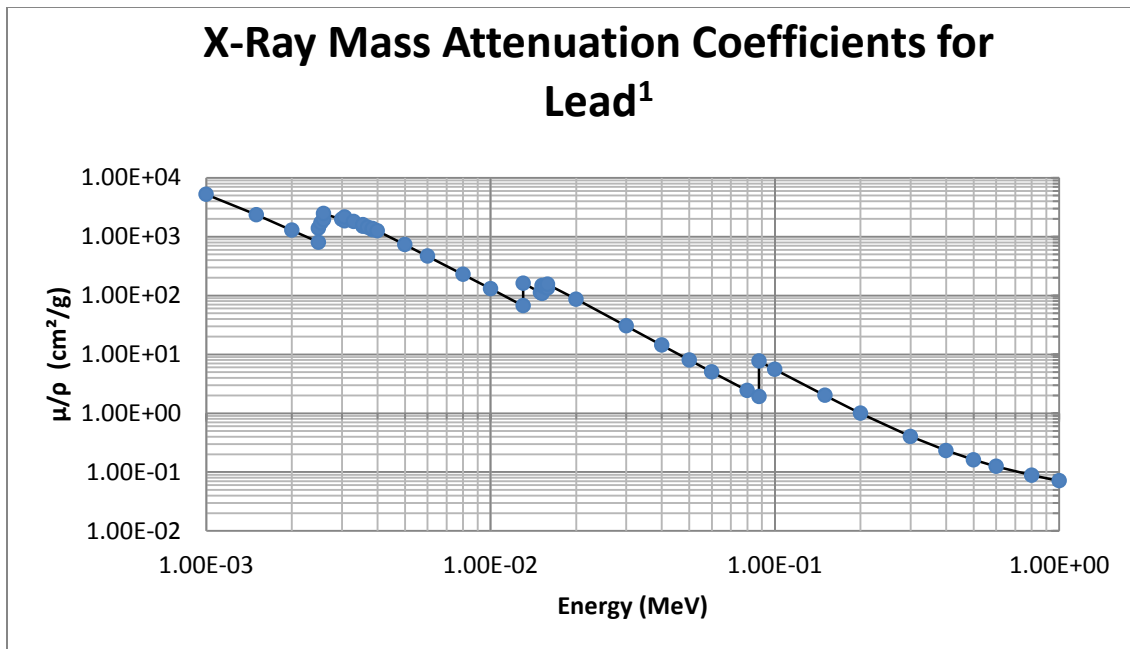


**Figure 4-1: X-Ray Mass Attenuation Coefficients for Lead (Hubbel, 2012)**

## 5.0 CONCLUSIONS

TLD's can accurately measure dose over a period of time and yield results which may give a broad picture of the radiological conditions of the environment in which the TLD is placed. However, if the radiological conditions of that environment change in the time in which the TLD is present, the result may not accurately represent the situation being measured. The experimental approach, using TLD's to measure dose distribution and the efficacy of the lead apron, was able to give a dose measurement which was representative of the room at the time of the experiment. Measurements using TLDs gave a realistic account of the dose over 24 h in the environment of the actinide facility. However, TLDs could not precisely and realistically measure the dose emitted only from an actinide oxide placed in the glovebox if the exposure in the room is not solely dependent on the actinide oxide in the glovebox. Therefore, the dose distribution may be skewed by other sources, such as other actinide oxides in the room, high terrestrial and cosmic background radiation, or contamination in the glovebox.

MCNP is a powerful tool for professionals in the field of radiation protection. MCNP uses a per particle history average to score tallies. By modeling and simulating the production, path, and interactions of millions, or as in this case, billions of particles, an MCNP user may measure radiological metrics, such as dose, in almost any conceivable radiological instance. Given enough particles for a specific geometry, MCNP can accurately estimate the dose to

individuals in radiological events. Utilizing MCNP therefore is an excellent method for simulating and observing the dose rate from a known source at an instant in time.

The room where the glovebox is located almost certainly has a higher background dose rate than zero, which is the assumption used in this model. Therefore, extremely low dose rates, such as those observed in the MCNP results for plutonium oxide and uranium oxide, in Tables 3-7 and 3-8, respectively, almost certainly pose a technical challenge when measured with a TLD. In particular, when dose rates from other sources in the room may be much greater than those caused by the presence of actinide oxides when they are in the glovebox, a TLD may not record data related to the presence of the actinide oxide. According to both the MCNP results, if a worker spends  $2000 \text{ h y}^{-1}$  working in front of the glovebox containing 25 g neptunium, or americium oxide, the annual dose received by the worker will be greater than 10% (500 mrem) of the  $5 \text{ rem y}^{-1}$  whole body limit (500 mrem is exceeded for both neptunium and americium oxide in 101 h and 345 h of work, respectively) to the whole body. However, if the worker is in front of a glovebox containing 25 g of plutonium or uranium oxide, the worker will not receive greater than 10% (500 mrem) of the limiting value (5 rem). Under ANSI/HPS N13.41-2011, multiple dosimetry would be necessary for the first two oxides.

Despite this, multiple dosimetry is not recommended for use at gloveboxes containing 25 g neptunium or americium oxide, despite the fact that the personal dose equivalent to any portion of the body has the potential to vary by 50% from the expected personal dose equivalent at the reference dosimeter location; and the personal dose equivalent has the potential to exceed 10% of the limiting value when a significant component of the effective dose from external sources

comes from a non-uniform radiation field (ANSI/HPS N13.41-2011). The reason for this is that with proper placement of the personnel dosimeter at the height of the glovebox middle window, which is approximately the area of the chest, the highest dose received by an individual from the source material in the glovebox will almost always be recorded. The ANSI/HPS standards support this idea stating, “Supplemental dosimeters shall be placed at body positions that permit assessment of the highest exposures, as determined from pre-job radiation surveys and evaluations of worker movement and position relative to the radiation source(s).” Since the detectors are placed on the front of the worker’s chest, this will provide a reasonable and generally overestimated dose equivalent to the worker’s torso. The dose rates at varying heights demonstrated in Figures 3-1 through 3-4 support this conclusion. The area of the chest contains many organs important when considering radiation dose, such as the lungs, breast, and stomach, which each have a tissue weighting factor of 0.12 in radiological protection (ICRP 2007). The tissues with high weighting factors are more important when considering dose because of the increased risk of radiation-induced carcinogenesis. Other areas of the “whole body” of concern, including the arms above the elbows and legs above the knee, will be overestimated by using a single TLD to measure whole body DDE, however, the estimate will conform to the purpose of the ANSI/HPS multiple dosimetry standard.

In light of this, further studies should be conducted utilizing TLD’s placed over a larger area to observe the dose rates to the whole body as defined by the NRC and DOE. Whicker et al, also came to a similar conclusion in their paper on a method to characterize photon radiation fields which was also done at the PF-4 plutonium facility. In the Whicker et al paper, the authors note that streaming through the gloveports may also contribute to dose rates at the glovebox.

Therefore, further considerations should be made to estimate if the arms above the elbow are receiving a higher dose than was estimated in this thesis.

## 6.0 REFERENCES

American National Standards Institute (ANSI). Criteria for Performing Multiple Dosimetry. Washington, DC: N13.41-2011. 2011.

Brown F.B., et al., MCNP™ Version 5, Los Alamos, NM: Los Alamos National Laboratory. LA-UR-02-3199. 2002.

Brookhaven National Laboratory (BNL) Nuclear Decay Data in the MIRD Format. Upton, NY.: Brookhaven National Laboratory (BNL). <http://www.nndc.bnl.gov/mird/> accessed October 16, 2012.

Baybarz, R.D. Preparation of Americium Dioxide by Thermal Decomposition of Americium Oxalate in Air. Oak Ridge, TN: Oak Ridge National Laboratory. (1960).

Department of Energy. Definitions 10 C.F.R. pt. 835.2. as last amended at 72FR 31926; 2007.

Department of Energy. Occupational Radiation Protection 10 C.F.R. pt. 835.202. as last amended at 72FR 31926; 2007.

Hiller L, et al., RadSrc. Livermore, CA. Lawrence Livermore National Laboratory. (2007).

Hoffman, J.M., Mallett, M. W. The LANL model 8823 whole body dosimeter and associated dose algorithm. Health Phys. 77():S96-S103; 1998.

International Commission on Radiological Protection (ICRP). Conversion Coefficients for Use in Radiological Protection against External Radiation, ICRP Publication 74, Annals of the ICRP 26 (3-4); 1996.

Knoll G.F., Radiation Detection and Measurement Edition 4. Hoboken, NJ: John Wiley & Sons; 2010.

Los Alamos National Security LLC. Glovebox Design . Los Alamos NM: Los Alamos National Laboratory; 2008. <http://engstandards.lanl.gov/specs.shtml> . Accessed October 22, 2012

Los Alamos National Security LLC. Glovebox Fabrication . Los Alamos NM: Los Alamos National Laboratory; 2008. <http://engstandards.lanl.gov/specs.shtml>. Accessed October 22, 2012

Los Alamos National Security LLC . Glovebox Gloves . Los Alamos NM: Los Alamos National Laboratory; 2008. <http://engstandards.lanl.gov/specs.shtml>. Accessed October 22, 2012

Morss, L.R.; Edelstein, N.M.; Fuger, J.; Katz, J.J. (Eds.) The Chemistry of the Actinide and Transactinide Elements, 4th ed., Dordrecht, The Netherlands: Springer. 2011

National Aeronautics and Space Administration (NASA). Space Flight Human-System Standard Volumes 1 Man-Systems Integration Standards Revision B. 1995. <http://msis.jsc.nasa.gov/> Accessed October 22 2012

Unger L.M. and Trubey D.K. Specific Gamma-Ray Dose Constants for Nuclides Important to Dosimetry and Radiological Assessment. Oak Ridge National Laboratory (ORNL) 1981.

Hubbell J. H. and Seltzer S. M. Tables of X-Ray Mass Attenuation Coefficients and Mass Energy-Absorption Coefficients from 1 keV to 20 MeV for Elements Z = 1 to 92 and 48 Additional Substances of Dosimetric Interest. Gaithersburg MD: National Institute of Standards and Technology. (1996). <http://www.nist.gov/pml/data/xraycoef/index.cfm>. Accessed October 22, 2012

Schwarz R. A., MCNP Visual Editor Version 24E. <http://mcnpvised.com/>. 2011.

Shultis JK. Report 290. Manhattan, KS: Engineering Experiment Station. College of Engineering Kansas State University. 2000.

Thermo Fischer Scientific© Product Overview: Materials and Assemblies for Thermoluminescence Dosimetry. <https://static.thermoscientific.com/images/D10472~.pdf> Accessed October 22, 2012

Whicker, J.J.; Borak, T.B.; Hsieh, F.H.; Hsu, H.H. A Method for Characterizing Photon Radiation Fields. Annual Health Physics Meeting. 1999.

X-5 Monte Carlo Team, MCNP™ – A General N-Particle Transport Code, Version 5 Volume I: Overview and Theory. Los Alamos, NM: Los Alamos National Laboratory (LANL), LA-UR-03-1987. 2003.

X-5 Monte Carlo Team, MCNP™ – A General N-Particle Transport Code, Version 5 Volume II: User's Guide, \. Los Alamos, NM: Los Alamos National Laboratory (LANL), LA-CP-03-0245. 2003.

Zoeger N, Brandl A. Dose Rate Distribution from a Standard Waste Drum Arrangement. Health Physics. 101(5):S142-S147, 2011.

## 7.0 APPENDIX A: MCNP INPUT WITH AMERICIUM OXIDE SOURCE

LANLAmBox

10 6 -7.9 -14 13 19 7 5 -6 #22 #30 #31 #28 #29 #37 imp:p=1  
12 6 -7.9 -7 8 -6 4 13 -14 imp:p=1  
13 6 -7.9 7 4 -3 -9 13 -14 imp:p=1  
14 6 -7.9 4 9 -10 19 13 -14 imp:p=1  
15 6 -7.9 -19 20 -10 -6 13 -14 #37 imp:p=1  
16 6 -7.9 16 -13 -10 8 19 -6 4 imp:p=1  
17 6 -7.9 -15 14 -10 8 19 -6 4 imp:p=1  
21 9 -2.23 11 -12 -5 1 -18 17 imp:p=1  
22 9 -2.23 17 -18 5 -6 11 -12 imp:p=1  
23 4 -4.36 -2 6 17 -18 11 -12 imp:p=1  
28 3 -1.27 -25 -6 5 imp:p=1  
29 3 -1.27 -26 -6 5 imp:p=1  
30 6 -7.9 -21 25 5 -6 imp:p=1  
31 6 -7.9 -22 26 5 -6 imp:p=1  
32 6 -7.9 20 -15 14 -19 -6 -10 imp:p=1  
33 6 -7.9 20 16 -13 -19 -6 -10 imp:p=1  
37 9 -2.23 -28 29 30 -31 20 -19 imp:p=1 \$ Borosilicate Safety Glass  
38 7 -1.19 -34 imp:p=1  
40 6 -7.9 -36 37 imp:p=1  
41 10 -11.32 -38 36 imp:p=1

42 6 -7.9 -39 38 imp:p=1

110 5 -3.0 -27 imp:p=1

118 10 -11.32 -41 imp:p=1

c

c

c

c TLD A

119 11 -1.050 -42 imp:p=1

120 0 -43 imp:p=1

121 0 -44 imp:p=1

122 11 -1.050 -45 imp:p=1

c

c TLD B

123 11 -1.050 -46 imp:p=1

124 0 -47 imp:p=1

125 0 -48 imp:p=1

126 11 -1.050 -49 imp:p=1

c

c TLD C

127 11 -1.050 -50 imp:p=1

128 0 -51 imp:p=1

129 0 -52 imp:p=1

130 11 -1.050 -53 imp:p=1

c

c TLD D

131 11 -1.050 -54 imp:p=1

132 0 -55 imp:p=1

133 0 -56 imp:p=1

134 11 -1.050 -57 imp:p=1

c

c TLD E

135 11 -1.050 -58 imp:p=1

136 0 -59 imp:p=1

137 0 -60 imp:p=1

138 11 -1.050 -61 imp:p=1

c

c TLD F

139 11 -1.050 -62 imp:p=1

140 0 -63 imp:p=1

141 0 -64 imp:p=1

142 11 -1.050 -65 imp:p=1

c

c TLD G

143 11 -1.050 -66 imp:p=1

144 0 -67 imp:p=1

145 0 -68 imp:p=1

146 11 -1.050 -69 imp:p=1

c

c TLD H

147 11 -1.050 -70 imp:p=1

148 0 -71 imp:p=1

149 0 -72 imp:p=1

150 11 -1.050 -73 imp:p=1

c

c TLD I

151 11 -1.050 -74 imp:p=1

152 0 -75 imp:p=1

153 0 -76 imp:p=1

154 11 -1.050 -77 imp:p=1

c

c TLD J

155 11 -1.050 -78 imp:p=1

156 0 -79 imp:p=1

157 0 -80 imp:p=1

158 11 -1.050 -81 imp:p=1

c

c

111 0 -9 7 3 13 -14 39 -40 imp:p=0 \$Inside Box Kill Zone

112 2 -0.0009 -37 27 imp:p=1

113 2 -0.0009 -5 -9 7 3 13 -14 19 39 40 #21 #28 #29

#30 #31 imp:p=1 \$Inside Box

114 2 -0.0009 -999 (-8:6:-20:10:-4:-16:15) #23 #38

#118 #119 #120 #121 #122 #123 #124 #125 #126 #127

#128 #129 #130 #131 #132 #133 #134 #135 #136

#137 #138 #139 #140 #141 #142 #143 #144 #145

#146 #147 #148 #149 #150 #151 #152 #153 #154

#155 #156 #157 #158

imp:p=1 \$inside universe

115 0 999 imp:p=0 \$Outside Universe

c Surface Cards

1 px 29.865

2 px 31.135

3 px -30

4 px -30.47265

5 px 30.02375

6 px 30.5

7 py 0

8 py -0.47625

9 py 70

10 py 70.47625

11 py 5

12 py 30

13 pz -40

14 pz 40

15 pz 40.47625

16 pz -40.47625

17 pz -7

18 pz 7

19 p -3.95 -1 0 -153.5

20 p -3.95 -1 0 -156.2  
 21 c/x 20 -19.05 10.16  
 22 c/x 20 19.05 10.16  
 24 px -15  
 25 rcc 30.5 20 -19.05 -44.95 0 0 10.11  
 26 rcc 30.5 20 19.05 -44.95 0 0 10.11  
 27 rcc 0 0.40 0 0 0.381765 0 3  
 28 py 68  
 29 py 40  
 30 pz -38  
 31 pz 38  
 32 p -3.95 -1 0 -153.5  
 33 p -3.95 -1 0 -156.2  
 34 rpp 33.18 47.18 0 40 -20 20  
 36 rcc 0 0.3175 0 0 3.15875 0 3.079375  
 37 rcc 0 0.396875 0 0 3.0 0 3.0  
 38 rcc 0 0.15875 0 0 3.47625 0 3.238125  
 39 rcc 0 0 0 0 3.79375 0 3.396875  
 40 px -5  
 41 rpp 32.2 32.25 0 40 -20 20  
 c  
 c  
 42 rpp 32.000 32.178 16 22 1 7 \$ ABS Backing A  
 43 rpp 31.962 32.0 16.5 21.5 3.5 5.0 \$ Element 1 TLD 700 A  
 44 rpp 31.962 32.0 16.5 21.5 1.5 3.0 \$ Element 4 TLD 400 A

45 rpp 31.258 31.962 16 22 1 7 \$ ABS Front A

c

c

46 rpp 32.000 32.178 16 22 -7 -1 \$ ABS Backing B

47 rpp 31.962 32.0 16.5 21.5 -3.0 -1.5 \$ Element 1 TLD 700 B

48 rpp 31.962 32.0 16.5 21.5 -5.0 -3.5 \$ Element 4 TLD 400 B

49 rpp 31.258 31.962 16 22 -7 -1 \$ ABS Front B

c

c

50 rpp 32.000 32.178 8 14 1 7 \$ ABS Backing C

51 rpp 31.962 32.0 8.5 13.5 3.5 5.0 \$ Element 1 TLD 700 C

52 rpp 31.962 32.0 8.5 13.5 1.5 3.0 \$ Element 4 TLD 400 C

53 rpp 31.258 31.962 8 14 1 7 \$ ABS Front C

c

c

54 rpp 32.000 32.178 8 14 -7 -1 \$ ABS Backing D

55 rpp 31.962 32.0 8.5 13.5 -3.0 -1.5 \$ Element 1 TLD 700 D

56 rpp 31.962 32.0 8.5 13.5 -5.0 -3.5 \$ Element 4 TLD 400 D

57 rpp 31.258 31.962 8 14 -7 -1 \$ ABS Front D

c

58 rpp 33.000 33.178 16 22 1 7 \$ ABS Backing E

59 rpp 32.962 33.0 16.5 21.5 3.5 5.0 \$ Element 1 TLD 700 E

60 rpp 32.962 33.0 16.5 21.5 1.5 3.0 \$ Element 4 TLD 400 E

61 rpp 32.258 32.962 16 22 1 7 \$ ABS Front E

c

c

62 rpp 33.000 33.178 16 22 -7 -1 \$ ABS Backing F

63 rpp 32.962 33.0 16.5 21.5 -3.0 -1.5 \$ Element 1 TLD 700 F

64 rpp 32.962 33.0 16.5 21.5 -5.0 -3.5 \$ Element 4 TLD 400 F

65 rpp 32.258 32.962 16 22 -7 -1 \$ ABS Front F

c

c

66 rpp 33.000 33.178 8 14 1 7 \$ ABS Backing G

67 rpp 32.962 33.0 8.5 13.5 3.5 5.0 \$ Element 1 TLD 700 G

68 rpp 32.962 33.0 8.5 13.5 1.5 3.0 \$ Element 4 TLD 400 G

69 rpp 32.258 32.962 8 14 1 7 \$ ABS Front G

c

c

70 rpp 33.000 33.178 8 14 -7 -1 \$ ABS Backing H

71 rpp 32.962 33.0 8.5 13.5 -3.0 -1.5 \$ Element 1 TLD 700 H

72 rpp 32.962 33.0 8.5 13.5 -5.0 -3.5 \$ Element 4 TLD 400 H

73 rpp 32.258 32.962 8 14 -7 -1 \$ ABS Front H

c

c

74 rpp 48.000 48.178 8 14 1 7 \$ ABS Backing I

75 rpp 47.962 48.0 8.5 13.5 3.5 5.0 \$ Element 1 TLD 700 I

76 rpp 47.962 48.0 8.5 13.5 1.5 3.0 \$ Element 4 TLD 400 I

77 rpp 47.258 47.962 8 14 1 7 \$ ABS Front I

c

78 rpp 48.000 48.178 8 14 -7 -1 \$ ABS Backing J

79 rpp 47.962 48.0 8.5 13.5 -3.0 -1.5 \$ Element 1 TLD 700 J

80 rpp 47.962 48.0 8.5 13.5 -5.0 -3.5 \$ Element 4 TLD 400 J

81 rpp 47.258 47.962 8 14 -7 -1 \$ ABS Front J

c

c

999 so 150

c Data Cards

nps 1000000000

c

c

c

c Air, Los Alamos 0.0009 g/cc

c

m2 6000.04p -0.000124

7014.04p -0.755268

8016.04p -0.231781

18000.04p -0.012827

c

c

c

c Hypalon - density = 1.27 g/cc

m3 6000.04p 6

1001.04p 12

17000.04p 2

8016.04p 2

16000.04p 1

c

c

c

c LX-57b Lead Glass 4.36 g/cc

m4 82000.04p -.5105759 \$Lead

14000.04p -.1589279 \$Silicon

56000.04p -.0447823932 \$Barium

5000.04p -.00931635 \$Boron

19000.04p -.0166296 \$Potassium

11023.04p -.00741857 \$Sodium

8000.04p -0.2523492868 \$ Oxygen

c

c Clear line g/cc

c Nuclide composition in ATOM FRACTION

c Reference: Louis Schulte

c m4 5010.04p 0.010556 \$ boron B10

c 5011.04p 0.042490 \$ boron B11

c 8016.04p 0.605569 \$ oxygen O16

c 8017.04p 0.000242 \$ oxygen O17

c 11023.04p 0.018333 \$ sodium Na23

c 13027.04p 0.005572 \$ aluminum Al27

c 14000.04p 0.191480 \$ silicon Si-nat

c 82000.04p 0.125758 \$ lead Pb-nat

c

c

c Americium Oxide Powder 3.0 g/cc Bulk Density

m5 95241 -0.85 8000 -0.15

c

c

c

c

c 304 SS - density = 8.0 g/cc

m6 6000.04p -0.0004

14000.04p -0.005

15000.04p -0.00023

16000.04p -0.00015

24000.04p -0.190

25000.04p -0.01

26000.04p -0.70173

28000.04p -0.0925

c

c

c

c

m7 \$ PMMA Lucite™ 1.19g/cm<sup>3</sup> NIST

1001.04p -0.080583

6012.04p -0.599884

8016.04p -0.319614

c

c

c

C Kapton Polyimide Film

m8 1000.04p -0.026326

6000.04p -0.681133

7000.04p -0.073270

8000.04p -0.209235

c

c

c

c

c

c

c

c Glass, Borosilicate (Pyrex), rho = 2.230

c

m9 5010.04p -7.933068e-3

5011.04p -3.213293e-2

8016.04p -0.539559

11023.04p -0.028191

13027.04p -0.011644

14000.04p -0.377220

19000.04p -0.003321

c

c

c

c

m10 82000.04p 1.0 \$Lead Pb-Nat

c

c

c

c

c ABS Plastic (C15H17N)n

m11 6000.04p 15

1000.04p 17

7000.04p 1

c

c

c Lithium Fluoride Enriched Li-7

m12 3007.04p -0.267585

9000.04p -0.732415

c

c

c

c Calcium Fluoride

m13 9000.04p -0.486659

20000.04p -0.513341

c

c

c

c

c

c SOURCE

sdef axs= 0 1 0

pos= 0 0.40 0

rad= D1

ext= D2

erg= D3

cel= 110

si1 H 0 3 \$ inner and outer radii

sp1 -21 1 \$ Default density proportional to 1

si2 H 0 0.381765 \$ Height

sp2 -21 0 \$ Default density constant with Y

c

c

c

C RadSource Run: Tue Apr 24 01:37:44 2012

C

C Input Isotopes

C Am-241 100%

C

C Total: 100%

C

C Age: 7.884e+008 s, 25 yrs

C Output Isotopes

C Tl-209 6.97515e-021% ( from Am-241 )

C Pb-209 2.86489e-017% ( from Am-241 )

C Bi-209 3.4074e-013% ( from Am-241 )

C Bi-213 6.69089e-018% ( from Am-241 )

C Po-213 1.00542e-026% ( from Am-241 )

C At-217 7.92739e-023% ( from Am-241 )

C Rn-217 1.58548e-028% ( from Am-241 )

C Fr-221 7.19337e-019% ( from Am-241 )

C Ra-225 3.14428e-015% ( from Am-241 )

C Ac-225 2.11397e-015% ( from Am-241 )

C Th-229 5.73373e-010% ( from Am-241 )

C Pa-233 1.34914e-007% ( from Am-241 )

C U-233 1.58378e-005% ( from Am-241 )

C Np-237 3.92158% ( from Am-241 )

C Am-241 96.0784% ( from Am-241 )

C

C Total: 100%

C 507 lines computed.

C Total Gamma Line Intensity: 9.51988e+010 ph/s/gm

C Total Bremsstrahlung Intensity: 0 ph/s/gm

C Total Intensity: 9.51988e+010 ph/s/gm

C Intensity of Unbinned lines is 0

C Intensity of Binned lines is 6.56388e+007

C Intensity of Bremsstrahlung 0

C Total intensity of all sources is 6.56388e+007

C =====

c SC 2 Energy boundries (MeV) for BINNED GAMMA LINES - 194 bins:

SI3 H 8.000000E-002 8.768000E-002 9.536000E-002 1.030400E-001  
1.107200E-001 1.184000E-001 1.260800E-001 1.337600E-001  
1.414400E-001 1.491200E-001 1.568000E-001 1.644800E-001  
1.721600E-001 1.798400E-001 1.875200E-001 1.952000E-001  
2.028800E-001 2.105600E-001 2.182400E-001 2.259200E-001  
2.336000E-001 2.412800E-001 2.489600E-001 2.566400E-001  
2.643200E-001 2.720000E-001 2.796800E-001 2.873600E-001  
2.950400E-001 3.027200E-001 3.104000E-001 3.180800E-001  
3.257600E-001 3.334400E-001 3.411200E-001 3.488000E-001  
3.564800E-001 3.641600E-001 3.718400E-001 3.795200E-001  
3.872000E-001 3.948800E-001 4.025600E-001 4.102400E-001  
4.179200E-001 4.256000E-001 4.332800E-001 4.409600E-001  
4.486400E-001 4.563200E-001 4.640000E-001 4.716800E-001  
4.793600E-001 4.870400E-001 4.947200E-001 5.024000E-001  
5.100800E-001 5.177600E-001 5.254400E-001 5.331200E-001  
5.408000E-001 5.484800E-001 5.561600E-001 5.638400E-001  
5.715200E-001 5.792000E-001 5.868800E-001 5.945600E-001  
6.022400E-001 6.099200E-001 6.176000E-001 6.252800E-001  
6.329600E-001 6.406400E-001 6.483200E-001 6.560000E-001  
6.636800E-001 6.713600E-001 6.790400E-001 6.867200E-001  
6.944000E-001 7.020800E-001 7.097600E-001 7.174400E-001  
7.251200E-001 7.328000E-001 7.404800E-001 7.481600E-001

7.558400E-001 7.635200E-001 7.712000E-001 7.788800E-001  
7.865600E-001 7.942400E-001 8.019200E-001 8.096000E-001  
8.172800E-001 8.249600E-001 8.326400E-001 8.403200E-001  
8.480000E-001 8.556800E-001 8.633600E-001 8.710400E-001  
8.787200E-001 8.864000E-001 8.940800E-001 9.017600E-001  
9.094400E-001 9.171200E-001 9.248000E-001 9.324800E-001  
9.401600E-001 9.478400E-001 9.555200E-001 9.632000E-001  
9.708800E-001 9.785600E-001 9.862400E-001 9.939200E-001  
1.001600E+000 1.009280E+000 1.016960E+000 1.024640E+000  
1.032320E+000 1.040000E+000 1.047680E+000 1.055360E+000  
1.063040E+000 1.070720E+000 1.078400E+000 1.086080E+000  
1.093760E+000 1.101440E+000 1.109120E+000 1.116800E+000  
1.124480E+000 1.132160E+000 1.139840E+000 1.147520E+000  
1.155200E+000 1.162880E+000 1.170560E+000 1.178240E+000  
1.185920E+000 1.193600E+000 1.201280E+000 1.208960E+000  
1.216640E+000 1.224320E+000 1.232000E+000 1.239680E+000  
1.247360E+000 1.255040E+000 1.262720E+000 1.270400E+000  
1.278080E+000 1.285760E+000 1.293440E+000 1.301120E+000  
1.308800E+000 1.316480E+000 1.324160E+000 1.331840E+000  
1.339520E+000 1.347200E+000 1.354880E+000 1.362560E+000  
1.370240E+000 1.377920E+000 1.385600E+000 1.393280E+000  
1.400960E+000 1.408640E+000 1.416320E+000 1.424000E+000  
1.431680E+000 1.439360E+000 1.447040E+000 1.454720E+000  
1.462400E+000 1.470080E+000 1.477760E+000 1.485440E+000  
1.493120E+000 1.500800E+000 1.508480E+000 1.516160E+000

1.523840E+000 1.531520E+000 1.539200E+000 1.546880E+000  
1.554560E+000 1.562240E+000 1.569920E+000

C

c SC 2 ASSOCIATED photon intensities (photons/sec/gm):

Sp3 D 0.000000E+000 1.584298E+005 1.276008E+005 5.250448E+007  
1.766184E+004 1.228709E+006 6.188106E+006 8.548751E+002  
7.359697E+003 5.642626E+005 1.252215E+005 1.304068E+004  
3.160457E+005 2.219590E+004 2.987035E+002 6.241819E+003  
1.658095E+004 9.672301E+005 1.951135E+003 5.116150E+004  
5.735154E+003 1.496362E+003 7.660048E+004 4.872524E+003  
1.406982E+003 4.658634E+004 8.039666E+003 1.351078E-005  
8.758362E+004 6.234801E+004 1.949010E+004 3.805799E+005  
1.851559E+005 1.802834E+005 6.489370E+005 0.000000E+000  
1.461757E+003 1.461757E+003 3.280427E+005 1.769563E+005  
3.435129E+004 7.186973E+003 1.191816E+004 1.705383E+003  
1.512304E+004 3.410767E+004 3.118415E+004 2.436269E+003  
4.263459E+003 1.473939E+004 4.385272E+003 3.532581E+003  
8.189445E-006 1.218131E+003 0.000000E+000 0.000000E+000  
0.000000E+000 4.567991E+003 1.096318E+003 4.237452E-006  
2.893604E-006 1.310311E-006 0.000000E+000 0.000000E+000  
2.074659E-006 1.218131E+003 1.827197E+003 3.410767E+003  
1.145043E+004 0.000000E+000 0.000000E+000 7.186973E+004  
6.821534E+002 1.534845E+003 8.648730E+003 4.592354E+004  
4.470541E+005 4.628898E+002 7.796039E+002 3.776206E+003  
4.105102E+004 6.090655E+003 1.474100E-006 7.796039E+003



0.000000E+000 0.000000E+000 0.000000E+000 0.000000E+000  
0.000000E+000 0.000000E+000 0.000000E+000 0.000000E+000  
0.000000E+000 0.000000E+000 8.968603E-004

C The integrated intensity for this input type is 6.563881E+007 Photons/s/gm

C

C

c

c

c

f4:p 120

fm4 1394266783

c Photon Fluence-to-Hp(10,0\*) dose conversion factors in an ICRP slab

c (ICRP 74 Tables A.1 and A.24)

c Energy units are MeV and conversion factor units are mrem/hr pps cm<sup>2</sup>.

de4 0.0100 0.0125 0.0150 0.0175 0.0200 0.0250 0.0300 0.0400 0.0500  
0.0600 0.0800 0.1000 0.1250 0.1500 0.2000 0.3000 0.4000 0.5000  
0.6000 0.8000 1.0000 1.5000 2.0000 3.0000 4.0000 5.0000 6.0000  
8.0000 10.0000

df4 2.40732E-05 1.86102E-04 2.96525E-04 3.84480E-04 3.69533E-04  
3.81615E-04 2.88631E-04 2.30116E-04 2.05350E-04 1.96844E-04  
2.10320E-04 2.41877E-04 2.96122E-04 3.46533E-04 4.59775E-04  
6.80119E-04 8.84520E-04 1.07614E-03 1.25346E-03 1.58080E-03  
1.87794E-03 2.51765E-03 3.07587E-03 4.00512E-03 4.85404E-03  
5.64282E-03 6.42776E-03 8.03196E-03 9.59904E-03

c

c

c

f14:p 121

fm14 1394266783

c Photon Fluence-to-Hp(10,0\*) dose conversion factors in an ICRP slab  
c (ICRP 74 Tables A.1 and A.24)

c Energy units are MeV and conversion factor units are mrem/hr pps cm<sup>2</sup>.

de14 0.0100 0.0125 0.0150 0.0175 0.0200 0.0250 0.0300 0.0400 0.0500  
0.0600 0.0800 0.1000 0.1250 0.1500 0.2000 0.3000 0.4000 0.5000  
0.6000 0.8000 1.0000 1.5000 2.0000 3.0000 4.0000 5.0000 6.0000  
8.0000 10.0000

df14 2.40732E-05 1.86102E-04 2.96525E-04 3.84480E-04 3.69533E-04  
3.81615E-04 2.88631E-04 2.30116E-04 2.05350E-04 1.96844E-04  
2.10320E-04 2.41877E-04 2.96122E-04 3.46533E-04 4.59775E-04  
6.80119E-04 8.84520E-04 1.07614E-03 1.25346E-03 1.58080E-03  
1.87794E-03 2.51765E-03 3.07587E-03 4.00512E-03 4.85404E-03  
5.64282E-03 6.42776E-03 8.03196E-03 9.59904E-03

c

c

c

c

c

f24:p 124

fm24 1394266783

c Photon Fluence-to-Hp(10,0\*) dose conversion factors in an ICRP slab

c (ICRP 74 Tables A.1 and A.24)

c Energy units are MeV and conversion factor units are mrem/hr pps cm<sup>2</sup>.

de24 0.0100 0.0125 0.0150 0.0175 0.0200 0.0250 0.0300 0.0400 0.0500  
0.0600 0.0800 0.1000 0.1250 0.1500 0.2000 0.3000 0.4000 0.5000  
0.6000 0.8000 1.0000 1.5000 2.0000 3.0000 4.0000 5.0000 6.0000  
8.0000 10.0000

df24 2.40732E-05 1.86102E-04 2.96525E-04 3.84480E-04 3.69533E-04  
3.81615E-04 2.88631E-04 2.30116E-04 2.05350E-04 1.96844E-04  
2.10320E-04 2.41877E-04 2.96122E-04 3.46533E-04 4.59775E-04  
6.80119E-04 8.84520E-04 1.07614E-03 1.25346E-03 1.58080E-03  
1.87794E-03 2.51765E-03 3.07587E-03 4.00512E-03 4.85404E-03  
5.64282E-03 6.42776E-03 8.03196E-03 9.59904E-03

c

c

c

c

f34:p 125

fm34 1394266783

c Photon Fluence-to-Hp(10,0\*) dose conversion factors in an ICRP slab

c (ICRP 74 Tables A.1 and A.24)

c Energy units are MeV and conversion factor units are mrem/hr pps cm<sup>2</sup>.

de34 0.0100 0.0125 0.0150 0.0175 0.0200 0.0250 0.0300 0.0400 0.0500  
0.0600 0.0800 0.1000 0.1250 0.1500 0.2000 0.3000 0.4000 0.5000  
0.6000 0.8000 1.0000 1.5000 2.0000 3.0000 4.0000 5.0000 6.0000  
8.0000 10.0000

df34 2.40732E-05 1.86102E-04 2.96525E-04 3.84480E-04 3.69533E-04  
3.81615E-04 2.88631E-04 2.30116E-04 2.05350E-04 1.96844E-04  
2.10320E-04 2.41877E-04 2.96122E-04 3.46533E-04 4.59775E-04  
6.80119E-04 8.84520E-04 1.07614E-03 1.25346E-03 1.58080E-03  
1.87794E-03 2.51765E-03 3.07587E-03 4.00512E-03 4.85404E-03  
5.64282E-03 6.42776E-03 8.03196E-03 9.59904E-03

c

c

c

c

f44:p 128

fm44 1394266783

c Photon Fluence-to-Hp(10,0\*) dose conversion factors in an ICRP slab

c (ICRP 74 Tables A.1 and A.24)

c Energy units are MeV and conversion factor units are mrem/hr pps cm<sup>2</sup>.

de44 0.0100 0.0125 0.0150 0.0175 0.0200 0.0250 0.0300 0.0400 0.0500  
0.0600 0.0800 0.1000 0.1250 0.1500 0.2000 0.3000 0.4000 0.5000  
0.6000 0.8000 1.0000 1.5000 2.0000 3.0000 4.0000 5.0000 6.0000  
8.0000 10.0000

df44 2.40732E-05 1.86102E-04 2.96525E-04 3.84480E-04 3.69533E-04  
3.81615E-04 2.88631E-04 2.30116E-04 2.05350E-04 1.96844E-04  
2.10320E-04 2.41877E-04 2.96122E-04 3.46533E-04 4.59775E-04  
6.80119E-04 8.84520E-04 1.07614E-03 1.25346E-03 1.58080E-03  
1.87794E-03 2.51765E-03 3.07587E-03 4.00512E-03 4.85404E-03  
5.64282E-03 6.42776E-03 8.03196E-03 9.59904E-03

c

c

c

c

f54:p 129

fm54 1394266783

c Photon Fluence-to-Hp(10,0\*) dose conversion factors in an ICRP slab

c (ICRP 74 Tables A.1 and A.24)

c Energy units are MeV and conversion factor units are mrem/hr pps cm<sup>2</sup>.

de54 0.0100 0.0125 0.0150 0.0175 0.0200 0.0250 0.0300 0.0400 0.0500

0.0600 0.0800 0.1000 0.1250 0.1500 0.2000 0.3000 0.4000 0.5000

0.6000 0.8000 1.0000 1.5000 2.0000 3.0000 4.0000 5.0000 6.0000

8.0000 10.0000

df54 2.40732E-05 1.86102E-04 2.96525E-04 3.84480E-04 3.69533E-04

3.81615E-04 2.88631E-04 2.30116E-04 2.05350E-04 1.96844E-04

2.10320E-04 2.41877E-04 2.96122E-04 3.46533E-04 4.59775E-04

6.80119E-04 8.84520E-04 1.07614E-03 1.25346E-03 1.58080E-03

1.87794E-03 2.51765E-03 3.07587E-03 4.00512E-03 4.85404E-03

5.64282E-03 6.42776E-03 8.03196E-03 9.59904E-03

c

c

c

c

f64:p 132

fm64 1394266783

c Photon Fluence-to-Hp(10,0\*) dose conversion factors in an ICRP slab  
c (ICRP 74 Tables A.1 and A.24)

c Energy units are MeV and conversion factor units are mrem/hr pps cm2.

de64 0.0100 0.0125 0.0150 0.0175 0.0200 0.0250 0.0300 0.0400 0.0500  
0.0600 0.0800 0.1000 0.1250 0.1500 0.2000 0.3000 0.4000 0.5000  
0.6000 0.8000 1.0000 1.5000 2.0000 3.0000 4.0000 5.0000 6.0000  
8.0000 10.0000

df64 2.40732E-05 1.86102E-04 2.96525E-04 3.84480E-04 3.69533E-04  
3.81615E-04 2.88631E-04 2.30116E-04 2.05350E-04 1.96844E-04  
2.10320E-04 2.41877E-04 2.96122E-04 3.46533E-04 4.59775E-04  
6.80119E-04 8.84520E-04 1.07614E-03 1.25346E-03 1.58080E-03  
1.87794E-03 2.51765E-03 3.07587E-03 4.00512E-03 4.85404E-03  
5.64282E-03 6.42776E-03 8.03196E-03 9.59904E-03

c

c

c

c

f74:p 133

fm74 1394266783

c Photon Fluence-to-Hp(10,0\*) dose conversion factors in an ICRP slab  
c (ICRP 74 Tables A.1 and A.24)

c Energy units are MeV and conversion factor units are mrem/hr pps cm2.

de74 0.0100 0.0125 0.0150 0.0175 0.0200 0.0250 0.0300 0.0400 0.0500  
0.0600 0.0800 0.1000 0.1250 0.1500 0.2000 0.3000 0.4000 0.5000  
0.6000 0.8000 1.0000 1.5000 2.0000 3.0000 4.0000 5.0000 6.0000

8.0000 10.0000

df74 2.40732E-05 1.86102E-04 2.96525E-04 3.84480E-04 3.69533E-04  
3.81615E-04 2.88631E-04 2.30116E-04 2.05350E-04 1.96844E-04  
2.10320E-04 2.41877E-04 2.96122E-04 3.46533E-04 4.59775E-04  
6.80119E-04 8.84520E-04 1.07614E-03 1.25346E-03 1.58080E-03  
1.87794E-03 2.51765E-03 3.07587E-03 4.00512E-03 4.85404E-03  
5.64282E-03 6.42776E-03 8.03196E-03 9.59904E-03

c

c

c

f84:p 136

fm84 1394266783

c Photon Fluence-to-Hp(10,0\*) dose conversion factors in an ICRP slab  
c (ICRP 74 Tables A.1 and A.24)

c Energy units are MeV and conversion factor units are mrem/hr pps cm<sup>2</sup>.

de84 0.0100 0.0125 0.0150 0.0175 0.0200 0.0250 0.0300 0.0400 0.0500  
0.0600 0.0800 0.1000 0.1250 0.1500 0.2000 0.3000 0.4000 0.5000  
0.6000 0.8000 1.0000 1.5000 2.0000 3.0000 4.0000 5.0000 6.0000  
8.0000 10.0000

df84 2.40732E-05 1.86102E-04 2.96525E-04 3.84480E-04 3.69533E-04  
3.81615E-04 2.88631E-04 2.30116E-04 2.05350E-04 1.96844E-04  
2.10320E-04 2.41877E-04 2.96122E-04 3.46533E-04 4.59775E-04  
6.80119E-04 8.84520E-04 1.07614E-03 1.25346E-03 1.58080E-03  
1.87794E-03 2.51765E-03 3.07587E-03 4.00512E-03 4.85404E-03  
5.64282E-03 6.42776E-03 8.03196E-03 9.59904E-03

c

f94:p 137

fm94 1394266783

c Photon Fluence-to-Hp(10,0\*) dose conversion factors in an ICRP slab

c (ICRP 74 Tables A.1 and A.24)

c Energy units are MeV and conversion factor units are mrem/hr pps cm<sup>2</sup>.

de94 0.0100 0.0125 0.0150 0.0175 0.0200 0.0250 0.0300 0.0400 0.0500  
0.0600 0.0800 0.1000 0.1250 0.1500 0.2000 0.3000 0.4000 0.5000  
0.6000 0.8000 1.0000 1.5000 2.0000 3.0000 4.0000 5.0000 6.0000  
8.0000 10.0000

df94 2.40732E-05 1.86102E-04 2.96525E-04 3.84480E-04 3.69533E-04  
3.81615E-04 2.88631E-04 2.30116E-04 2.05350E-04 1.96844E-04  
2.10320E-04 2.41877E-04 2.96122E-04 3.46533E-04 4.59775E-04  
6.80119E-04 8.84520E-04 1.07614E-03 1.25346E-03 1.58080E-03  
1.87794E-03 2.51765E-03 3.07587E-03 4.00512E-03 4.85404E-03  
5.64282E-03 6.42776E-03 8.03196E-03 9.59904E-03

c

c

c

f104:p 140

fm104 1394266783

c Photon Fluence-to-Hp(10,0\*) dose conversion factors in an ICRP slab

c (ICRP 74 Tables A.1 and A.24)

c Energy units are MeV and conversion factor units are mrem/hr pps cm<sup>2</sup>.

de104 0.0100 0.0125 0.0150 0.0175 0.0200 0.0250 0.0300 0.0400 0.0500

0.0600 0.0800 0.1000 0.1250 0.1500 0.2000 0.3000 0.4000 0.5000  
0.6000 0.8000 1.0000 1.5000 2.0000 3.0000 4.0000 5.0000 6.0000  
8.0000 10.0000

df104 2.40732E-05 1.86102E-04 2.96525E-04 3.84480E-04 3.69533E-04  
3.81615E-04 2.88631E-04 2.30116E-04 2.05350E-04 1.96844E-04  
2.10320E-04 2.41877E-04 2.96122E-04 3.46533E-04 4.59775E-04  
6.80119E-04 8.84520E-04 1.07614E-03 1.25346E-03 1.58080E-03  
1.87794E-03 2.51765E-03 3.07587E-03 4.00512E-03 4.85404E-03  
5.64282E-03 6.42776E-03 8.03196E-03 9.59904E-03

c

c

c

f114:p 141

fm114 1394266783

c Photon Fluence-to-Hp(10,0\*) dose conversion factors in an ICRP slab

c (ICRP 74 Tables A.1 and A.24)

c Energy units are MeV and conversion factor units are mrem/hr pps cm<sup>2</sup>.

de114 0.0100 0.0125 0.0150 0.0175 0.0200 0.0250 0.0300 0.0400 0.0500  
0.0600 0.0800 0.1000 0.1250 0.1500 0.2000 0.3000 0.4000 0.5000  
0.6000 0.8000 1.0000 1.5000 2.0000 3.0000 4.0000 5.0000 6.0000  
8.0000 10.0000

df114 2.40732E-05 1.86102E-04 2.96525E-04 3.84480E-04 3.69533E-04  
3.81615E-04 2.88631E-04 2.30116E-04 2.05350E-04 1.96844E-04  
2.10320E-04 2.41877E-04 2.96122E-04 3.46533E-04 4.59775E-04  
6.80119E-04 8.84520E-04 1.07614E-03 1.25346E-03 1.58080E-03

1.87794E-03 2.51765E-03 3.07587E-03 4.00512E-03 4.85404E-03  
5.64282E-03 6.42776E-03 8.03196E-03 9.59904E-03

c

c

c

c

c

f124:p 144

fm124 1394266783

c Photon Fluence-to-Hp(10,0\*) dose conversion factors in an ICRP slab

c (ICRP 74 Tables A.1 and A.24)

c Energy units are MeV and conversion factor units are mrem/hr pps cm<sup>2</sup>.

de124 0.0100 0.0125 0.0150 0.0175 0.0200 0.0250 0.0300 0.0400 0.0500  
0.0600 0.0800 0.1000 0.1250 0.1500 0.2000 0.3000 0.4000 0.5000  
0.6000 0.8000 1.0000 1.5000 2.0000 3.0000 4.0000 5.0000 6.0000  
8.0000 10.0000

df124 2.40732E-05 1.86102E-04 2.96525E-04 3.84480E-04 3.69533E-04  
3.81615E-04 2.88631E-04 2.30116E-04 2.05350E-04 1.96844E-04  
2.10320E-04 2.41877E-04 2.96122E-04 3.46533E-04 4.59775E-04  
6.80119E-04 8.84520E-04 1.07614E-03 1.25346E-03 1.58080E-03  
1.87794E-03 2.51765E-03 3.07587E-03 4.00512E-03 4.85404E-03  
5.64282E-03 6.42776E-03 8.03196E-03 9.59904E-03

c

c

c

c

f134:p 145

fm134 1394266783

c Photon Fluence-to-Hp(10,0\*) dose conversion factors in an ICRP slab

c (ICRP 74 Tables A.1 and A.24)

c Energy units are MeV and conversion factor units are mrem/hr pps cm<sup>2</sup>.

de134 0.0100 0.0125 0.0150 0.0175 0.0200 0.0250 0.0300 0.0400 0.0500  
0.0600 0.0800 0.1000 0.1250 0.1500 0.2000 0.3000 0.4000 0.5000  
0.6000 0.8000 1.0000 1.5000 2.0000 3.0000 4.0000 5.0000 6.0000  
8.0000 10.0000

df134 2.40732E-05 1.86102E-04 2.96525E-04 3.84480E-04 3.69533E-04  
3.81615E-04 2.88631E-04 2.30116E-04 2.05350E-04 1.96844E-04  
2.10320E-04 2.41877E-04 2.96122E-04 3.46533E-04 4.59775E-04  
6.80119E-04 8.84520E-04 1.07614E-03 1.25346E-03 1.58080E-03  
1.87794E-03 2.51765E-03 3.07587E-03 4.00512E-03 4.85404E-03  
5.64282E-03 6.42776E-03 8.03196E-03 9.59904E-03

c

c

c

c

f144:p 148

fm144 1394266783

c Photon Fluence-to-Hp(10,0\*) dose conversion factors in an ICRP slab

c (ICRP 74 Tables A.1 and A.24)

c Energy units are MeV and conversion factor units are mrem/hr pps cm<sup>2</sup>.

de144 0.0100 0.0125 0.0150 0.0175 0.0200 0.0250 0.0300 0.0400 0.0500  
0.0600 0.0800 0.1000 0.1250 0.1500 0.2000 0.3000 0.4000 0.5000  
0.6000 0.8000 1.0000 1.5000 2.0000 3.0000 4.0000 5.0000 6.0000  
8.0000 10.0000

df144 2.40732E-05 1.86102E-04 2.96525E-04 3.84480E-04 3.69533E-04  
3.81615E-04 2.88631E-04 2.30116E-04 2.05350E-04 1.96844E-04  
2.10320E-04 2.41877E-04 2.96122E-04 3.46533E-04 4.59775E-04  
6.80119E-04 8.84520E-04 1.07614E-03 1.25346E-03 1.58080E-03  
1.87794E-03 2.51765E-03 3.07587E-03 4.00512E-03 4.85404E-03  
5.64282E-03 6.42776E-03 8.03196E-03 9.59904E-03

c

c

c

c

f154:p 149

fm154 1394266783

c Photon Fluence-to-Hp(10,0\*) dose conversion factors in an ICRP slab  
c (ICRP 74 Tables A.1 and A.24)

c Energy units are MeV and conversion factor units are mrem/hr pps cm<sup>2</sup>.

de154 0.0100 0.0125 0.0150 0.0175 0.0200 0.0250 0.0300 0.0400 0.0500  
0.0600 0.0800 0.1000 0.1250 0.1500 0.2000 0.3000 0.4000 0.5000  
0.6000 0.8000 1.0000 1.5000 2.0000 3.0000 4.0000 5.0000 6.0000  
8.0000 10.0000

df154 2.40732E-05 1.86102E-04 2.96525E-04 3.84480E-04 3.69533E-04  
3.81615E-04 2.88631E-04 2.30116E-04 2.05350E-04 1.96844E-04

2.10320E-04 2.41877E-04 2.96122E-04 3.46533E-04 4.59775E-04  
6.80119E-04 8.84520E-04 1.07614E-03 1.25346E-03 1.58080E-03  
1.87794E-03 2.51765E-03 3.07587E-03 4.00512E-03 4.85404E-03  
5.64282E-03 6.42776E-03 8.03196E-03 9.59904E-03

c

c

c

c

f164:p 152

fm164 1394266783

c Photon Fluence-to-Hp(10,0\*) dose conversion factors in an ICRP slab

c (ICRP 74 Tables A.1 and A.24)

c Energy units are MeV and conversion factor units are mrem/hr pps cm<sup>2</sup>.

de164 0.0100 0.0125 0.0150 0.0175 0.0200 0.0250 0.0300 0.0400 0.0500

0.0600 0.0800 0.1000 0.1250 0.1500 0.2000 0.3000 0.4000 0.5000

0.6000 0.8000 1.0000 1.5000 2.0000 3.0000 4.0000 5.0000 6.0000

8.0000 10.0000

df164 2.40732E-05 1.86102E-04 2.96525E-04 3.84480E-04 3.69533E-04

3.81615E-04 2.88631E-04 2.30116E-04 2.05350E-04 1.96844E-04

2.10320E-04 2.41877E-04 2.96122E-04 3.46533E-04 4.59775E-04

6.80119E-04 8.84520E-04 1.07614E-03 1.25346E-03 1.58080E-03

1.87794E-03 2.51765E-03 3.07587E-03 4.00512E-03 4.85404E-03

5.64282E-03 6.42776E-03 8.03196E-03 9.59904E-03

c

c

c

c

f174:p 153

fm174 1394266783

c Photon Fluence-to-Hp(10,0\*) dose conversion factors in an ICRP slab

c (ICRP 74 Tables A.1 and A.24)

c Energy units are MeV and conversion factor units are mrem/hr pps cm<sup>2</sup>.

de174 0.0100 0.0125 0.0150 0.0175 0.0200 0.0250 0.0300 0.0400 0.0500  
0.0600 0.0800 0.1000 0.1250 0.1500 0.2000 0.3000 0.4000 0.5000  
0.6000 0.8000 1.0000 1.5000 2.0000 3.0000 4.0000 5.0000 6.0000  
8.0000 10.0000

df174 2.40732E-05 1.86102E-04 2.96525E-04 3.84480E-04 3.69533E-04  
3.81615E-04 2.88631E-04 2.30116E-04 2.05350E-04 1.96844E-04  
2.10320E-04 2.41877E-04 2.96122E-04 3.46533E-04 4.59775E-04  
6.80119E-04 8.84520E-04 1.07614E-03 1.25346E-03 1.58080E-03  
1.87794E-03 2.51765E-03 3.07587E-03 4.00512E-03 4.85404E-03  
5.64282E-03 6.42776E-03 8.03196E-03 9.59904E-03

c

c

c

f184:p 156

fm184 1394266783

c Photon Fluence-to-Hp(10,0\*) dose conversion factors in an ICRP slab

c (ICRP 74 Tables A.1 and A.24)

c Energy units are MeV and conversion factor units are mrem/hr pps cm<sup>2</sup>.

de184 0.0100 0.0125 0.0150 0.0175 0.0200 0.0250 0.0300 0.0400 0.0500  
0.0600 0.0800 0.1000 0.1250 0.1500 0.2000 0.3000 0.4000 0.5000  
0.6000 0.8000 1.0000 1.5000 2.0000 3.0000 4.0000 5.0000 6.0000  
8.0000 10.0000

df184 2.40732E-05 1.86102E-04 2.96525E-04 3.84480E-04 3.69533E-04  
3.81615E-04 2.88631E-04 2.30116E-04 2.05350E-04 1.96844E-04  
2.10320E-04 2.41877E-04 2.96122E-04 3.46533E-04 4.59775E-04  
6.80119E-04 8.84520E-04 1.07614E-03 1.25346E-03 1.58080E-03  
1.87794E-03 2.51765E-03 3.07587E-03 4.00512E-03 4.85404E-03  
5.64282E-03 6.42776E-03 8.03196E-03 9.59904E-03

c

f194:p 157

fm194 1394266783

c Photon Fluence-to-Hp(10,0\*) dose conversion factors in an ICRP slab

c (ICRP 74 Tables A.1 and A.24)

c Energy units are MeV and conversion factor units are mrem/hr pps cm<sup>2</sup>.

de194 0.0100 0.0125 0.0150 0.0175 0.0200 0.0250 0.0300 0.0400 0.0500  
0.0600 0.0800 0.1000 0.1250 0.1500 0.2000 0.3000 0.4000 0.5000  
0.6000 0.8000 1.0000 1.5000 2.0000 3.0000 4.0000 5.0000 6.0000  
8.0000 10.0000

df194 2.40732E-05 1.86102E-04 2.96525E-04 3.84480E-04 3.69533E-04  
3.81615E-04 2.88631E-04 2.30116E-04 2.05350E-04 1.96844E-04  
2.10320E-04 2.41877E-04 2.96122E-04 3.46533E-04 4.59775E-04  
6.80119E-04 8.84520E-04 1.07614E-03 1.25346E-03 1.58080E-03  
1.87794E-03 2.51765E-03 3.07587E-03 4.00512E-03 4.85404E-03

5.64282E-03 6.42776E-03 8.03196E-03 9.59904E-03

c

c

mode p